GCAGS JOURNAL
A Publication of the Gulf Coast Association of Geological Societies
www.gcags.org

Stratigraphic Architecture of the Shelf-to-Intrashelf Basin Transition along the Northern Margin of the Late Albian Maverick Intrashelf Basin, Lower Pecos River Canyon, Southwestern Texas

Jeffrey Sitgreaves[1,2] and Charles Kerans[1,3]

[1]*John A. and Katherine G. Jackson School of Geosciences, Department of Geological Sciences, University of Texas at Austin, 1 University Station C1100, Austin, Texas 78712, U.S.A.*

[2]*ExxonMobil Upstream Business Development, 22777 Springwoods Village Pkwy., Spring, Texas 77389, U.S.A.*

[3]*Bureau of Economic Geology, Jackson School of Geosciences, University of Texas at Austin, University Station, Box X, Austin, Texas 78713–8924, U.S.A.*

ABSTRACT

The geomorphic expression of intrashelf basin systems and their associated facies patterns is extremely subtle, with shelf-to-basin dip angles that can average 0.3° across a 50 km slope profile. This presents an issue to stratigraphers working to understand facies variability at the reservoir-scale because the changes in stratal geometries at the shelf-to-basin transition will occur beneath the resolution of conventional subsurface datasets. In order to address this issue, outcrops that capture the shelf-to-basin transition from the late Albian (Cretaceous) Maverick intrashelf basin were mapped along a 15 km dip-oriented transect on the Lower Pecos River. This study takes a quantitative approach to characterize the relationships between dip angles, paleobathymetry, and sediment production along the shelf-to-basin profile. The goal of this research is to provide detailed documentation of an intrashelf basin that can function as an outcrop analog for fields producing from similar reservoir settings by improving the understanding of facies variability away from the wellbore.

Exposures along the Pecos River Canyon provides a unique opportunity to observe the transition from grain-dominated facies of the ramp crest into planktonic foraminifera mudstones-wackestones of the intrashelf basin. For this study, 475 m of detailed sections were collected at five localities and integrated with a high-resolution 3D digital outcrop model to document the relationship between vertical facies successions and stratal geometries of the intrashelf basin profile. The development of the differential topography and facies changes associated with the formation of the late Albian Maverick intrashelf basin is attributed to differential sediment accumulation rates between active rudist-skeletal shoal formation, versus deeper-water foraminiferal mudstones of the basin-center. Rudist bank deposition early in the Albian 6 Composite Sequence formed the positive topographic relief (1–3 m) that led to the localization of rapid shallow-water sediment accumulation. After the development of subtle topographic expressions, ensuing changes in relative sea level promoted the development at the margins that were dominated by rudist faunal assemblages. Shallow-water basin margins consist of either lagoon-inlet-barrier or foreshore-shoreface depositional environments with upper shoreface-foreshore facies demonstrating that the platform built to sea level. Within the same stratigraphic interval, skeletal wackestones and foram mudstones are deposited in an intrashelf basin setting. The location of a paleo-shoreline and faunal assemblages within the same high-frequency sequence allows for the estimation that the total shelf-to-basin relief of the Maverick intrashelf basin was greater than 50 m. The forced regressive highstand deposits of the Albian 21 high-frequency sequence form the final phase of high-progradation-rate basin filling. These prograding shoreface deposits downlap the condensed mud-rich intrashelf basin facies of the Albian 19 and 20 high-frequency sequences, and infill the topography formed by the differential aggradation of the intrashelf basin margins.

Manuscript received April 1, 2020; revised manuscript received July 6, 2020; manuscript accepted July 10, 2020.

GCAGS Journal, v. 10 (2021), p. 76–96.

The primary goal of this study, is to capture a change in stratal geometry at the shelf-to-basin transition and lateral shift of facies from grain-dominated facies on the ramp into mud-dominated intrashelf basin deposits for the Albian 19 and 20 high-frequency sequences. The extensive and largely undeformed exposures along the Lower Pecos River Canyon and adjacent Amistad Reservoir highlight this transition and

provide clear evidence for the constructional differential-accumulation-driven formation for the late Albian Maverick intrashelf basin. Similar constructional progressions have been called on for the Bab intrashelf basin and the Natih 'E' Formation in the Cretaceous of the Middle East.

INTRODUCTION

Intrashelf basins are carbonate depositional systems that are characteristic of broad carbonate platforms that form in greenhouse settings. The development of intrashelf basin systems occurs on the platform-top, protected behind the shallow platform rim (Read, 1985, 1998). Intrashelf basin systems can be summarized as geologically short-lived basins that are shallow features (50–150 m water depth), and reach several hundred kilometers across (Burchette and Wright, 1992). Intrashelf basin depositional systems host some of the most prolific hydrocarbon systems in the world (e.g, Jurassic-Cretaceous of the Arabian Plate). Intrashelf basins are efficient and self-contained depositional systems where significant accumulations of organic-rich mudrocks occur on the broad shelf top, immediately adjacent to potentially high-quality carbonate reservoir facies (Murris, 1984; Van Buchem et al., 2002b; Ziegler, 2001). The development of broad carbonate shelfs in greenhouse climate regimes creates the ideal setting for intrashelf basin development. However, intrashelf basins have been characterized throughout the geologic record. The earliest examinations of intrashelf basins was conducted in the Cambrian Nolichucky Formation by Markello and Read (1981) and the Jurassic Abenaki Formation documented by Eliuk (1978). The most investigated intrashelf basins are located on the Arabian Plate; studies include the Jurassic Hanifa Formation (Droste, 1990; Murris, 1984; Ziegler, 2001), the Aptian Bab intrashelf basin (Alsharhan, 1985; Van Buchem et al., 2002a) and the Cenomanian Mishrif-Savark-Natih Formation (Burchette, 1993; Droste and Van Steenwinkel, 2004; Razin et al., 2010; Van Buchem et al., 2002b). Several intrashelf basins have been identified on the Cretaceous Comanche Platform in the Northwest Gulf of Mexico, investigations include the Maverick intrashelf basin (Kerans et al., 1995; Rose, 1972), and the Fort Stockton intrashelf basin (Zahm, 1997). Most recently, Bourget et al. (2013) has proposed evidence for the Quaternary Maltia intrashelf basin in NW Australia, which is the first documented example of a Cenozoic intrashelf basin system.

Intrashelf basins typically have an origin that is constructional, meaning that basin formation is driven by differential sedimentation rates that develop across the carbonate factory, while receiving little input from tectonics or compaction. The constructional development of intrashelf basins raises several questions about the main drivers behind the origin and the specific controls driving the differential sedimentation rates that influence the evolution of these systems (Van Buchem et al., 2002b). In particular, what is the ability of the carbonate factory to develop a topographic response to eustatic fluctuations and ecoeustatic drivers? How can relatively subtle topographic expression lead to the complete shut-down of carbonate productivity in the basin-center? What factors influence the deposition and preservation of organic-rich source rocks within intrashelf basins?

The goal of this study is to provide detailed documentation on the shelf-to-basin evolution of the late Albian Maverick intrashelf basin across four high-frequency sequences that record the changing profile. Quantifying the change in stratal geometries and component facies allows improved understanding of the dynamic profile of intrashelf basin systems. The shelf-to-basin transition is marked by a gradually changing depositional profile

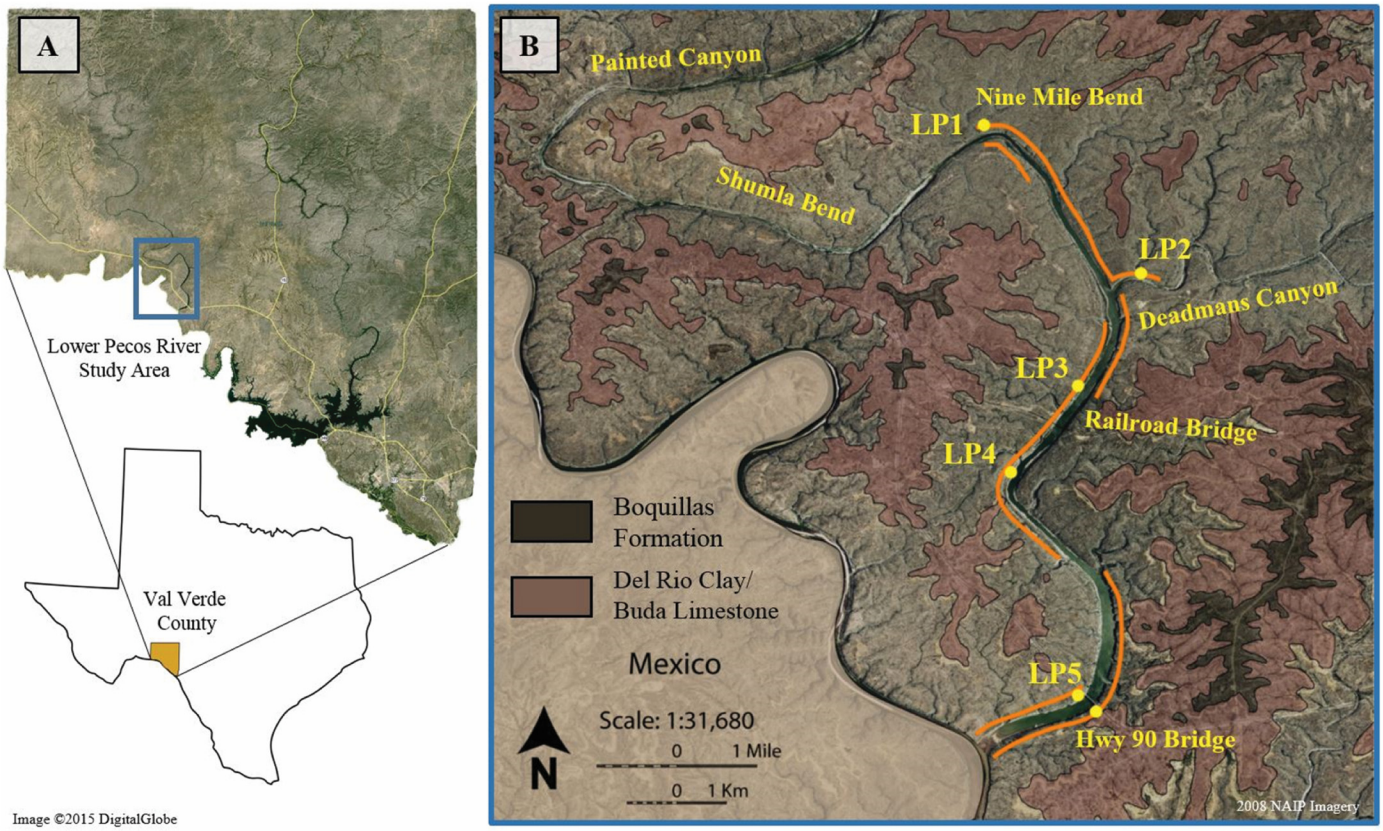

Figure 1. Location of the Lower Pecos River Canyon in Val Verde County, Texas (blue box). Interpretation of the Del Rio–Buda composite unit and the Boquillas (Eagle Ford) Formation based on National Agriculture Imagery Program (NAIP) aerial imagery. Included on the base map are the location of key landmarks, the five measured sections (yellow dots), and digital outcrop model (orange lines).

and associated lateral shifts in carbonate skeletal grainstone and mudstone deposits. The exposures along the lower 15 km of the Pecos River in western Val Verde County (Fig. 1) provide evidence of low-angle (0.3°) clinoforms and downlap of grainstones onto basin-centered mudstones of the Maverick intrashelf basin. The Pecos River Canyon is ideal for this investigation because (1) it offers a rare opportunity to trace the shelf-to-basin transition of a carbonate ramp depositional system from the inner ramp into intrashelf basin deposits, (2) it provides continuous exposures with manageable accessibility, (3) the outcrop-scale is on the order of subsurface reservoirs (50 km of nearly-continuous dip profile), and (4) it has the ability to serve as an analog for reservoirs producing from rudist margins surrounded by mudstone deposits on the shelf-top.

Outcrop analog modeling for reservoir characterization is an important research approach that can provide insight to stratal geometric relationships in subsurface reservoirs that can be difficult to recognize with typical subsurface data (Kerans et al., 1994). The motivation behind the development of outcrop analogs is to build an understanding of the depositional system and facies patterns at the inter-well scale to help reduce uncertainty for reservoir modeling in carbonate environments (Howell et al., 2014; Kerans and Tinker, 1997). The late Albian Maverick intrashelf basin is an excellent outcrop analog to reservoirs that produce from similar rudist-bearing facies that rim the Aptian Bab intrashelf basin (e.g, Bu Hasa fields and Al Huwaisah; Van Buchem et al., 2002a; Yose et al., 2006), and has similarities with intrashelf basin system development in the Cenomanian Natih Formation (Alsharhan, 1995; Van Buchem et al., 2002b). The outcrop study of the Maverick intrashelf basin provides documentation of the changes in depositional facies that are linked to changing stratal geometries at the high-frequency-sequence scale. This facies-stratal geometry link improve our ability to predict the distribution of high-energy grain-dominated facies and their mud-dominated intrashelf basin system counterparts in the subsurface.

GEOLOGIC AND STRATIGRAPHIC SETTING

The exposures of the late Albian Maverick intrashelf basin are situated on the Comanche Shelf, protected behind the Stuart City reef trend that rimmed the ancestral Gulf of Mexico (Fig. 1) (Bebout and Loucks, 1974; Lehmann et al., 1998; Rose, 1972; Wilson, 1975; Winker and Buffler, 1988). The presence of localized Salmon Peak facies of skeletal wackestones/mudstones behind the Stuart City reef trend occurs frequently across the continuous Albian (Cretaceous) shelf, that spanned from Mexico to Florida (Salvador, 1991; Waite, 2009; Winker and Buffler, 1988). Across Texas, there were three active intrashelf basin depositional systems during the Early Cretaceous; the Maverick intrashelf basin, Fort Stockton intrashelf basin, and the East Texas intrashelf basin (Fig. 2). These three intrashelf basin systems highlight two very distinct styles of intrashelf basin origin and duration. The Maverick intrashelf basin and the Fort Stockton intrashelf basin were geologically short-lived basins that evolved as a result of differential sediment accumulation rates, where sedimentation along the ramp margin was greater than sedimentation in the basin, creating differential topography. During the late Albian, the East Texas Basin can also be considered an intrashelf basin with mudstones deposited behind the Stuart City margin. The style of the East Texas intrashelf basin contrasts significantly to that of the Maverick and Ft. Stockton intrashelf basin systems. The East Texas Basin formed as the result of a failed rift in the Jurassic that occurred north of the main rift system that formed the Gulf of Mexico, and the presence of salt influences sedimentation throughout the Cretaceous (Jackson and Seni, 1983). Other key structural elements that impact sedimentation in the northwestern Gulf of Mexico are a series of uplifts and tectonic lows including the Llano Uplift, Sabine Arch, Coahuilla Platform, San Marcos Arch, and the Sabinas Basin (Salvador, 1991). Sediment distribution across the late Albian Comanche Shelf is highlighted by the distribution of shallow platform sediments, grain-dominated rudist margins, and mud-dominated intrashelf basin deposits with respect to the reef tend of Stuart City shelf margin that separates the shelf from the ancestral Gulf of Mexico (Lehmann et al., 2000; Osleger et al., 2004; Rose, 1972; Smith et al., 2000; Winker and Buffler, 1988) (Fig. 2) .

Regional Stratigraphy

In the northwestern Gulf of Mexico the first-order tectono-eustatic rise is characterized by the transition from evaporites and clastic-dominated facies assemblages in the Jurassic to carbonate-dominated facies throughout the Cretaceous (Bebout and Loucks, 1974). There are four Cretaceous supersequences (K1–K4) identified in the basin. (Goldhammer, 1991; Goldhammer and Johnson, 1999) . Within these four supersequences, Phelps et al. (2014) identified seven composite sequences from the Hauterivian through the early Campanian that frame the shelf architecture of the Comanche Shelf along the San Marcos Arch. Deposition within the Albian can be further divided into six shorter-duration composite sequences capturing the final stage of Albian deposition and highlighted in the outcrops along the Pecos River. The youngest Albian composite sequence is composed of six high-frequency sequences (Kerans et al., 1995). The Albian 18–21 high-frequency sequences comprise the Albian 6 composite sequence, which characterize deposition of the final highstand episode of the K2 supersequence. The final stage of deposition of the Maverick intrashelf basin is marked by the backstepping Albian 22 and 23 high-frequency sequences, and compose the initial transgressive deposits within the K3 supersequence. (Figs. 3 and 4)

The Albian 6 Composite Sequence

The Washita Group composes the Albian 6 composite sequence. It overlies the Fredericksburg Group and the Glen Rose Formation. At the end of Fredericksburg time (Albian 5 composite sequence; Albian 17 high-frequency sequence) sedimentation led to the formation of a fully-aggraded flat-topped platform. Evidence for complete basin aggradation is highlighted by the deposition of tidal flat and evaporate facies of the Fort Terrett Formation over distal facies within the Maverick Basin during Glen Rose (early Albian) time (Kerans et al., 1995; Lehmann et al., 1998). The next major stage of development is a transgression that caused rudist buildup assemblages formerly centered on the Stuart City Margin to step nearly 150 km landward of the margin onto the Devils River Uplift (Kerans, 2002; Lehmann et al., 1998; Winker and Buffler, 1988). This event formed the margins of the northern Maverick intrashelf basin, and defined as the Devils River Trend (Webster, 1980). During this major transgression, focused sediment accumulation, aggradation, and progradation created margins with positive topographic relief and a broad area of deeper water and slower sedimentation—the late Albian Maverick intrashelf basin. After the establishment of the ramp margin around the Maverick intrashelf basin there was a final period of progradation during wich grainstone deposition stepped seaward more than 30 km. This episode of progradation can be observed along the northern and western margins of the late Albian intrashelf basin (Kerans et al., 1995; Osleger et al., 2004).

One of the earliest investigations of the Devils River–Salmon Peak formations along the Lower Pecos River was by Lozo and Smith (1964) was to define the lithostratigraphic terminology. Other studies have continued to make observations of lateral facies relationships and environmental interpretations across much of the Comanche Platform (Rose, 1972; Smith,

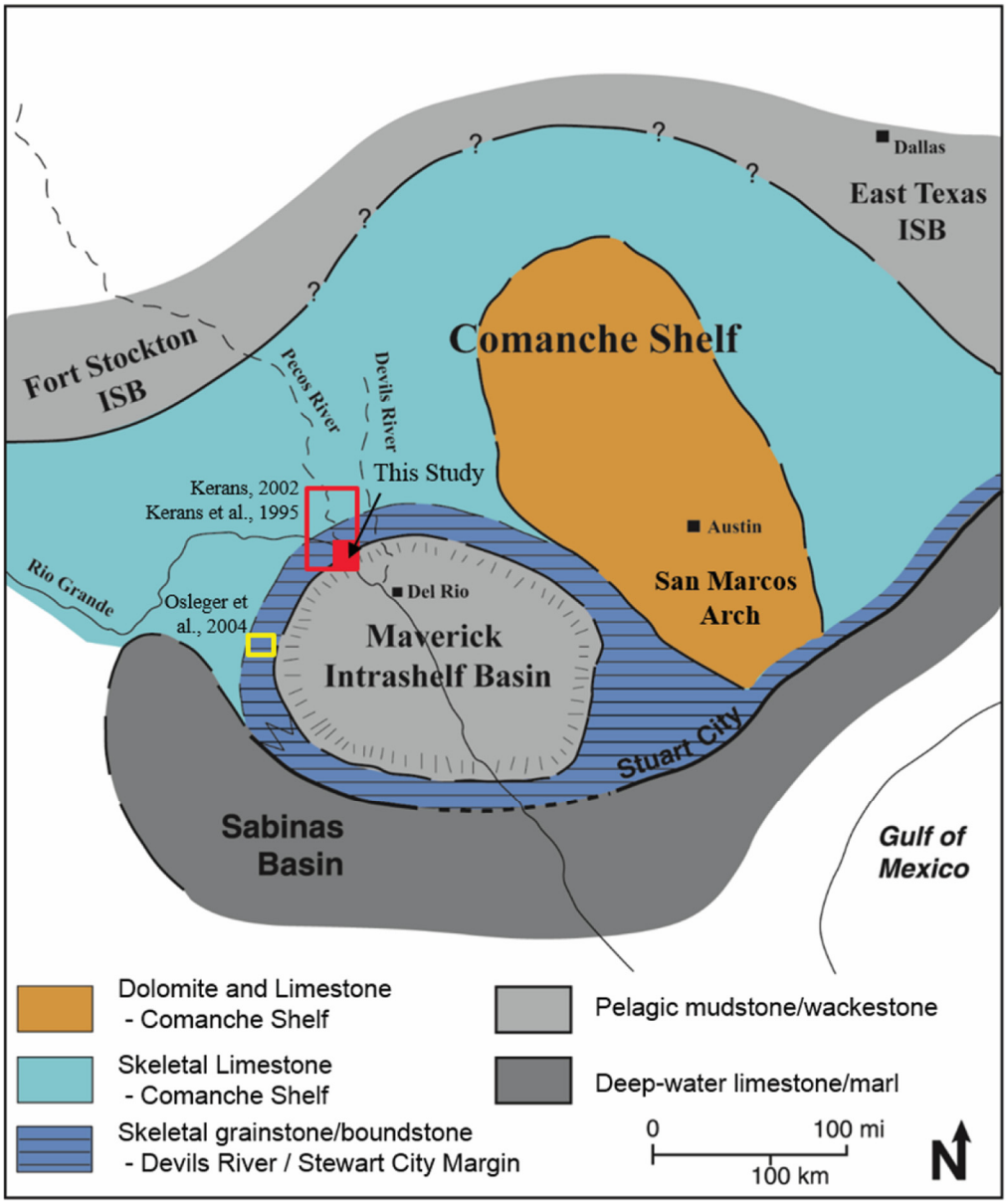

Figure 2. Paleogeographic map for the late Albian of the Comanche shelf in the northwestern Gulf of Mexico. Note the location of three intrashelf basins (intrashelf basin systems) on the shelf-top; Maverick intrashelf basin, Fort Stockton intrashelf basin, and the East Texas intrashelf basin. Study location is highlighted by the red box along the northern margin of the Maverick Intrashelf Basin. Modified after Osleger (2004), Rose, (1974), Smith (2000), Waite (2009), and Winker and Buffler, (1988).

1981; Smith et al., 2000). Based on an extensive field investigation along the Pecos River, Kerans et al. (1995) defined the high-resolution sequence stratigraphic framework for the late Albian Maverick intrashelf basin by tracing high-frequency sequence boundaries across nearly 50 km of dip-oriented exposures. The established framework consists of six high-frequency sequences (Albian 18–23 high-frequency sequences), and includes depositional environments of the ramp system that range from peritidal inner ramp to intrashelf basin (Fig. 3). The first four high-frequency sequence represent deposition of the Albian 6 composite sequence and sedimentation in the Albian is completed with the backstepping sequences of the Albian 22 and 23 high-frequency sequences. The Albian 18–23 high-frequency sequences (Devils River–Salmon Peak formations) are overlain unconformably by the Del Rio Clay and Buda Limestone. The lithostratigraphic terminology developed by Lozo and Smith (1964) that was later revised by Rose (1972) can be compared and placed into the sequence stratigraphic framework constructed by Kerans et al. (1995) (Fig. 4).

DATA AND METHODS

The methodology used for this study includes (1) standard field-based outcrop mapping and collection of measured sections, (2) acquisition of ground-based Global Navigation Satellite System (GNSS)–calibrated photographs used for the construction of a digital outcrop model (DOM) utilizing the latest photogrammetry techniques (commercial software: Agisoft), (3) Integration of vertical sections with the dense point clouds to map key high-frequency sequence boundaries (commercial software: QT Modeler), and (4) stratigraphic modeling using a refinement gridding process combined with set conformance rules and modeled within a stratigraphic framework package (commercial software: Landmark DecisionSpace).

Outcrop-Based Sections-Facies Characterization

Five measured sections totaling 475 m were collected along a dip-transect at an average spacing of 1.5 km along the Lower

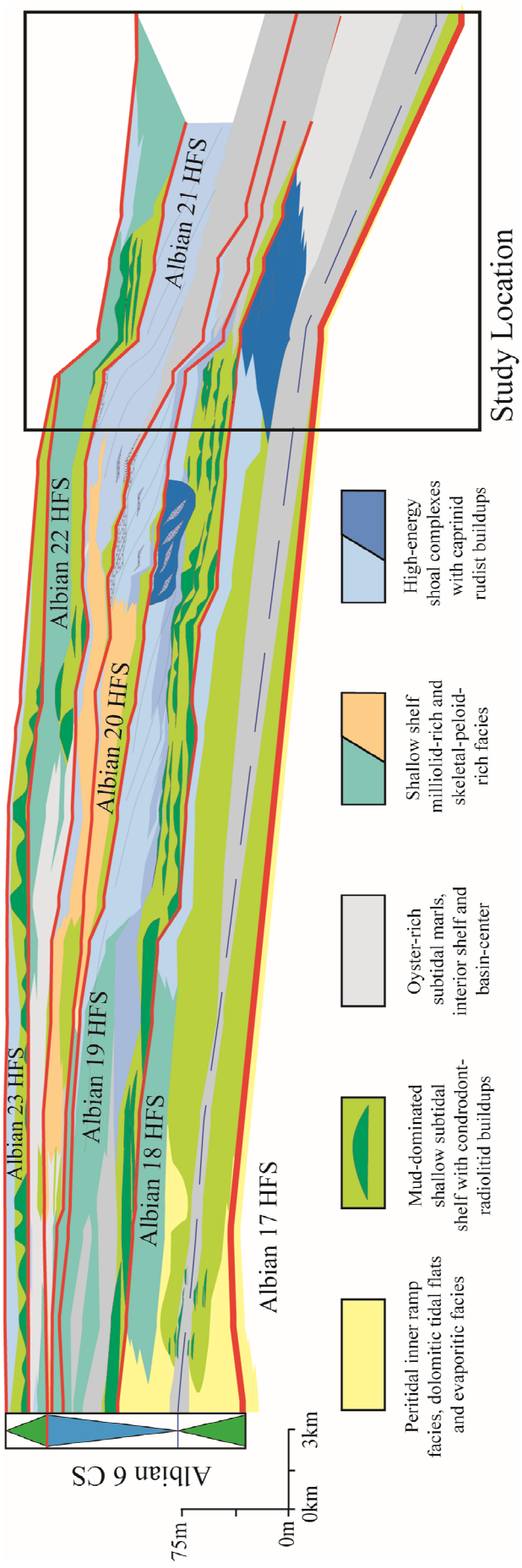

Figure 3. Late Albian high-resolution sequence stratigraphic framework showing the six high-frequency sequences, and the relationship between facies tracts and systems tracts. The focus for this study along the Lower Pecos River is indicated by the black box. Modified after Kerans (2002).

Pecos River Canyon (LPR1–LPR5) (Fig. 1). Sections were logged at a 20 cm resolution following the correlation and stratigraphic analysis methods outlined in detail by Kerans and Tinker (1997). Additionally, 110 hand samples and a series of outcrop photographs were collected to verify the field descriptions of lithofacies (using the Dunham classification; Dunham, 1962), weathering, sedimentary structures, and bedding characteristics. From the collected hand samples, 25 thin sections were taken along a vertical transect of the LPR4 measured section (Fig. 1) to provide petrographic documentation of facies including the important condensed intrashelf basin facies within the Albian 19 and 20 high-frequency sequences.

This research builds upon the sequence stratigraphic framework that was established by Kerans et al., (1995) and modified later in Kerans (2002), in a study that collected a series of 35 measured sections across a 50 km dip-oriented transect of the Pecos River. The sequence stratigraphic principles of this study follow models initially developed for siliciclastic sequences by (Mitchum and Van Wagoner, 1991; Vail, 1987; Van Wagoner et al., 1990) and further modified for applications in carbonates environments by (Handford and Loucks, 1993; Kerans and Tinker, 1997). The sequence hierarchy and carbonate ramp environment terminologies will follow those established by Burchette and Wright (1992) and modified by Kerans and Fitchen (1995).

Three-Dimensional Digital Outcrop Modeling (Photogrammetry Techniques)

The evolution of digital outcrop modeling techniques has been fueled by the need to process large field-scale datasets, allow for advanced visualization, and provide the ability to quantify depositional geometries and geobodies that can serve as analog inputs into subsurface reservoir models. Perhaps the most revolutionary advance in digital outcrop modeling was the development and application of lidar for use in outcrop characterization by Bellian et al. (2005). Pringle et al., (2006) conducted a review of a variety of methods (including lidar and photogrammetry) for digital outcrop modeling and for studying outcrop analogs. Early work with photogrammetry used a small number of aerial photographs to create georegistered orthophotomosaics and low-resolution digital surface models (4 m resolution) (Pringle et al., 2004). Modern photogrammetry methods use a series of overlapping photographs taken at a variety of different angles, with precise camera orientations/locations to create high-resolution 3D point clouds. In the last few years, there has been significant improvements in terrestrial photogrammetric methods that allow for digital outcrop models that are comparable to lidar accuracies, and have clear advantages over lidar with significant decreases in cost and acquisition time and the integration of red-green-blue (RGB) data to the point cloud. Photogrammetry combined with aerial perspectives obtained from unmanned aerial vehicles (UAV) have become the standard for quantitative outcrop characterization.

For the construction of high-resolution digital outcrop models on the Lower Pecos River, over 800 outcrop photographs were collected. Time stamped location tracks were collected with a backpack-mounted Trimble Pro 6H Receiver and post-processed differential GNSS (DGNSS) was used to get submeter horizontal and vertical accuracies. The photographs were captured using a Sony A7R (36 megapixel) camera with a Canon EF

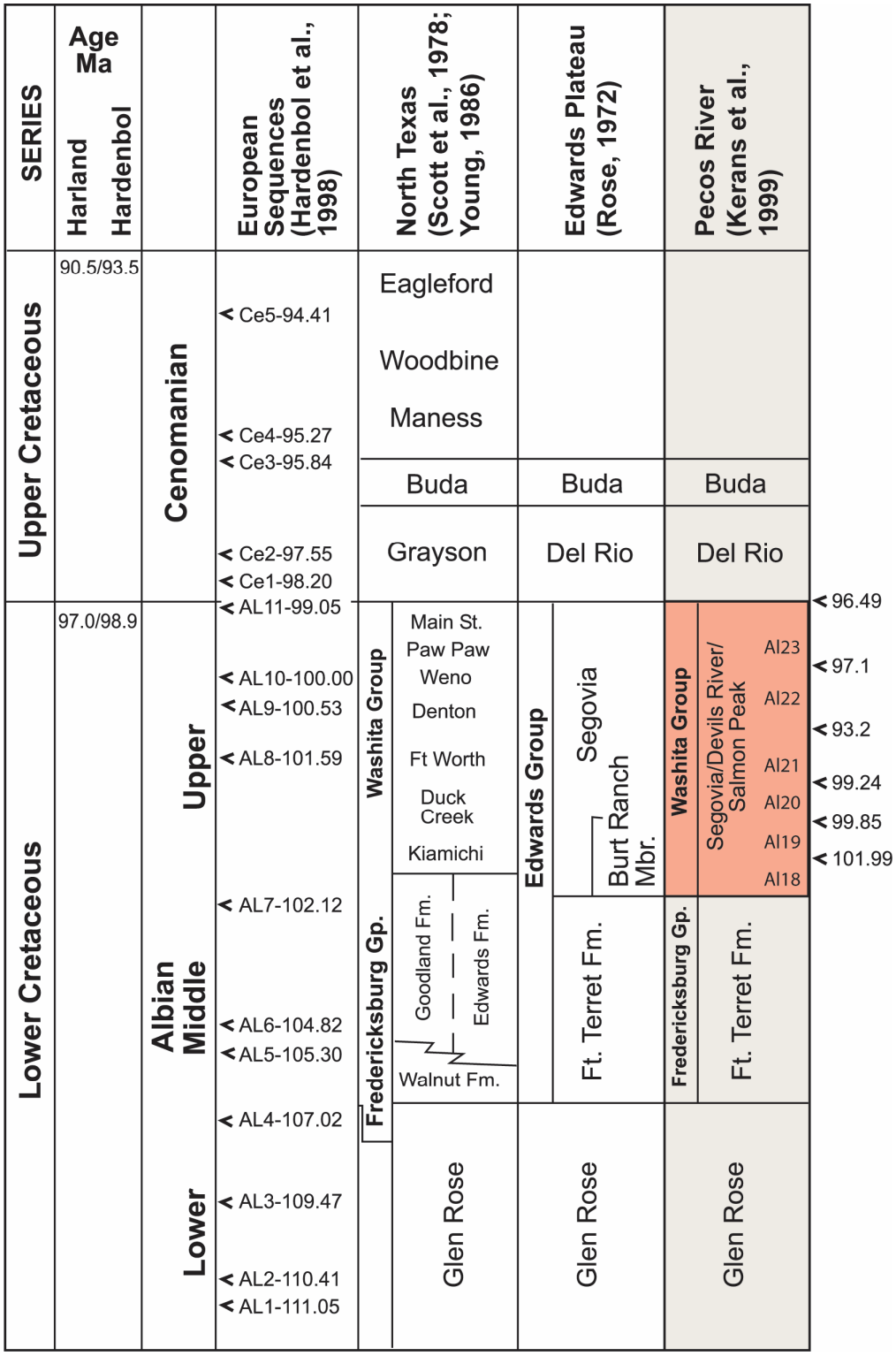

Figure 4. Stratigraphic column of the Pecos River study area, showing the relationship of the high-frequency sequence stratigraphy to lithostratigraphic terminology and highlighting key age constraints for the six Albian high-frequency sequences (modified after Kerans, 2002; Scott and Kerans 2002). The area of focus for this study is marked in red.

24–105 mm lens attached to a monopod. Camera locations were obtained by synchronizing the timestamps of the DGNSS tracts with the camera, and then correcting for the offset between the receiver and camera position. The integration of location with the outcrop photographs significantly decreases field acquisition time by several hours and processing time by days. Three-dimensional outcrop models were constructed using Agisoft Photoscan® software on a workstation. The DOM construction process is computer intensive with typical model run times that take over 30 hours to complete despite a robust CPU/RAM workstation configuration. Resolutions obtained by using terrestrial based photogrammetric methods on the Lower Pecos River were 2 cm/pixel with a 1.5 m average camera location error (x, y, z). The high-resolution digital outcrop model provides the ability to accurately interpret the subtle depositional dips of the shelf to intrashelf basin profile that range from 0.1 to 0.7°. Examples of the acquisition, processing, interpretation and modeling stages of this study are provided in Figure 5.

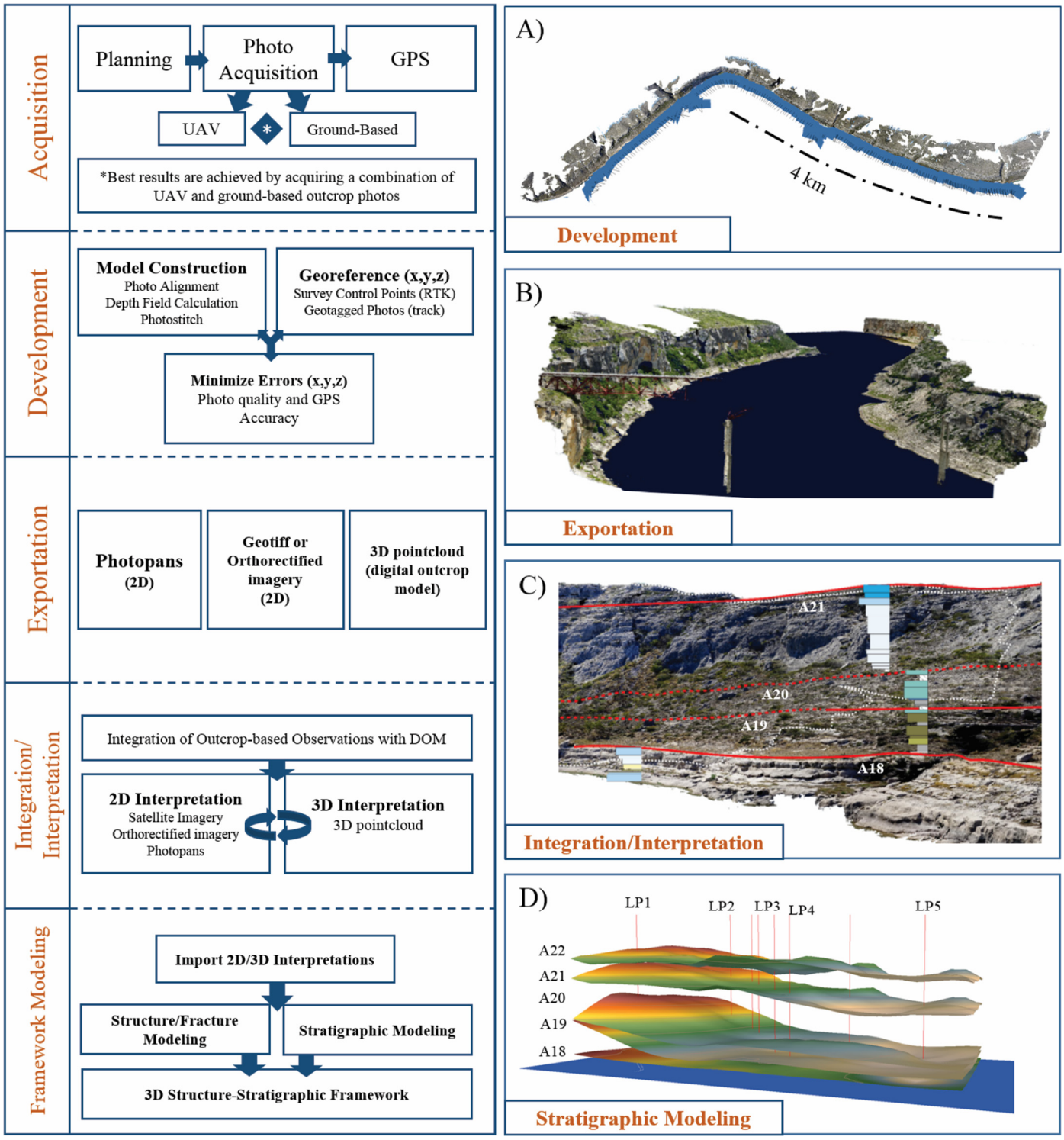

Figure 5. Construction of a digital outcrop model (DOM) from acquisition through interpretation. The export and interpretation of 3D point clouds presents the opportunity to model outcrop-mapped surfaces into a high-resolution 3D framework. (A) Development of a digital outcrop model using photogrammetry; 250 photographs were used to create a dense point cloud with over 400,000,000 points. (B) Dense 3D point cloud at the Highway 90 Bridge with 2 cm/pixel resolution. (C) Integration of the LP4 measured section with the point cloud that guided the interpretation of the high-frequency sequence boundaries. D) Stratigraphic framework using interpretations from the digital outcrop model and 5 measured sections. Modified after Zahm and Kerans (2014).

Interpretation and Stratigraphic Modeling

The interpretation of a high-density point cloud requires specialized software that is designed to handle multi-million point datasets (model sizes are roughly equivalent to a field-scale 3D seismic survey). The interpretation of this outcrop model focused on the Albian 18–22 high-frequency sequences along the Lower Pecos River Canyon. The interpretations were made using field-based tracing of the sequence boundaries and integrating these with vertical measured sections. Interpretations were then propagated on the 3D DOM across the 9 km section of the Lower Pecos River. These interpretations were then exported from a visualization based software and into Landmark's DecisionSpace® software package for the construction of a three-dimensional stratigraphic framework for the Albian 18–22 high-frequency sequences.

FACIES ASSOCIATIONS AND DEPOSITIONAL MODEL

There are 23 lithofacies assemblages that characterize depositional patterns across the carbonate ramp profile of the Pecos River. (Kerans et al., 1995). These facies can be further subdivided into four facies tracts based on distinct sediment supply/water depth/energy regimes. The key facies tracts of the Albian 6 composite sequence include the (1) peritidal inner ramp, (2) mud-dominated shallow subtidal, (3) high-energy shoal complex, and (4) the intrashelf basin (Kerans, 2002). The paleoecology of rudist-bearing deposits of the Comanche shelf has been of much interest, including a focus on Albian rudist reef communities (Scott, 1990) as well as a focus on rudist buildups in the Devils River Formation (Scott and Kerans, 2004). Rudist distribution, type, and associated sediment bodies were integrated into a sequence stratigraphic framework by Kerans (2002) who demonstrated the strong partitioning of rudist assemblages and facies exists between the highstand and transgressive systems tract of the last six Albian high-frequency sequences.

The facies tracts observed in this study along the Lower Pecos River are dominated by high-energy shoal complexes and down-dip intrashelf basin deposits. The high-energy shoal complexes are strongly progradational with upward-coarsening foreshore-shoreface deposits. The Albian 19 deposits in the updip section of this study also contain well-developed mud-dominated shallow subtidal shelf environments. These three facies tracts and key lithofacies assemblages are discussed in further detail below.

High-Energy Shoal Complex Facies Tract

Facies assemblages in this facies tract are dominated by caprinid-skeletal grainstones and rudstones that are indicative of wave agitation, mechanical breakdown of grains, and winnowing of mud, leaving a well-sorted skeletal sand facies. Sedimentary structures include burrows, low-angle parallel current lamination, 5–10 cm thick planar-tabular crossbed sets, and in the upper portions of the facies assemblage, small-scale trough cross-stratification oriented at high-angle to the seaward dipping swash-laminated foreshore deposits. The sedimentary structures indicate at the shoreline of the profile help to constrain depositional models. Variations of the depositional settings was documented by Kerans et al., (1995) and Kerans (2002) between tidally dominated and wave-dominated facies successions for each of the high-frequency sequences. These high-energy deposits occur at the ramp crest and grade laterally offshore into skeletal grain-dominated packstones, before transitioning into intrashelf basin facies. Three key lithofacies of the shoal complex facies tract are described below:

Caprinid-Peloidal-Skeletal Grainstone (Figs. 6A and 6B): This facies consist of swash-laminated grainstone fabrics. The accretion stratified bedding dips seaward at 2-3° and the grains are well-sorted medium-grained size sand. The clasts are primarily composed of peloids, forminifera (miliolids), skeletal fragments (including caprinids, mollusks, and echinoderms), and rarer large (5-10 cm) caprinid fragments. Peloids are well-rounded, and skeletal fragments are highly abraded with thin micritic rims. This facies passes downdip into trough cross-stratified peloid-skeletal grainstones (Kerans, 2002).

Caprinid Rudstone (Fig. 6C): This facies is characterized by massive bedding with intact ~30 cm caprinid rudist and gravel-sized caprinid fragments. Matrix consists of coarse-sand to gravel-sized skeletal fragments that include rudists and mollusks. The coarse sand and skeletal fragments are well-rounded with micritc rims. Abundant peloids and intraclasts grains are observed around caprinid rudist. The original aragonite that composed the caprinid shells has been completely replaced by blocky calcite cement. This facies passes vertically into trough cross-stratified grainstones, and transitions downdip into cross-bedded grain-dominated packstones (Kerans et al., 1995).

Peloidal-Skeletal Grain-dominated Packstone (Fig. 6D): This facies is composed fine- to medium-grained sand size peloids and skeletal clasts with tabular crossbed sets that are 5–10 cm thick. There is a major abundance of fine-sand sized moderately rounded peloids and intraclasts. Skeletal clasts are predominantly rudist and mollusk fragments with well-developed micritic envelops. Moldic porosity is common and develops from late-stage fabric-selective dissolution of grains. This facies passes laterally into more distal heavily bioturbated peloid-skeletal mud-dominated packstones (Kerans et al., 1995).

Mud-Dominated Shallow Subtidal Facies Tract

The distinct facies within the mud-dominated shallow-subtidal shelf facies tract are dominated by toucasid-radiolitid assemblages. This unit forms both biostromal complexes that extend hundreds of meters to bioherms that range between 50–150 m in diameter with well-developed flank beds (Kerans, 2002). The primary facies assemblages can be divided into bedded miliolid-gastropod grainstones and mound/intramound facies. Downdip from the well-developed bioherms there is a distinct contrast and change in mound development. Mound facies assemblages on the Lower Pecos River are predominantly massive toucasid rudstones that form 2–4 m biostromes. Three levels of mound development can be identified at Nine-Mile Bend (LP1; Fig. 1) with primary mound builders of toucasid rudists. Occasionally, these mounds are capped by thin monopleurid rudstones and are surrounded by gastropod-miliolid packstones to toucasid skeletal packstones. The shallow subtidal facies tract in the outer ramp passes laterally into skeletal wackestones and mudstones in the intrashelf basin. The two key facies assemblages of the mud-dominated outer ramp deposits are discussed below:

Toucasid Rudstone: Massive weathered toucasid rudstones that form biostromal 2–4 m mounds and are predominantly composed of large 10–20 cm toucasid rudists. These rudstones contain the largest observed toucasid rudists along the entire depositional profile of the Maverick intrashelf basin. The toucasid rudists are intact with dark brown thin wall structures. The matrix of this rudstone is a fine-grained mud-dominated fabric. This mounded facies assemblages is typically capped by bedded miliolid grainstones/packstones and passes downdip into a toucasid gastropod mud-dominated packstones (Kerans et al., 1995).

Toucasid Gastropod Packstone: Thin- to medium-bedded mud-dominated packstone/wackestone that is composed of toucasid rudists and high-spired gastropods. The matrix is fine grained and mud-dominated with an abundance of miliolid formanifera. The toucasid rudists are a diagnostic fauna of the mud-dominated shallow subtidal facies tract. Toucasid rudists are typically 10 cm in diameter with thin dark brown peanut-shaped

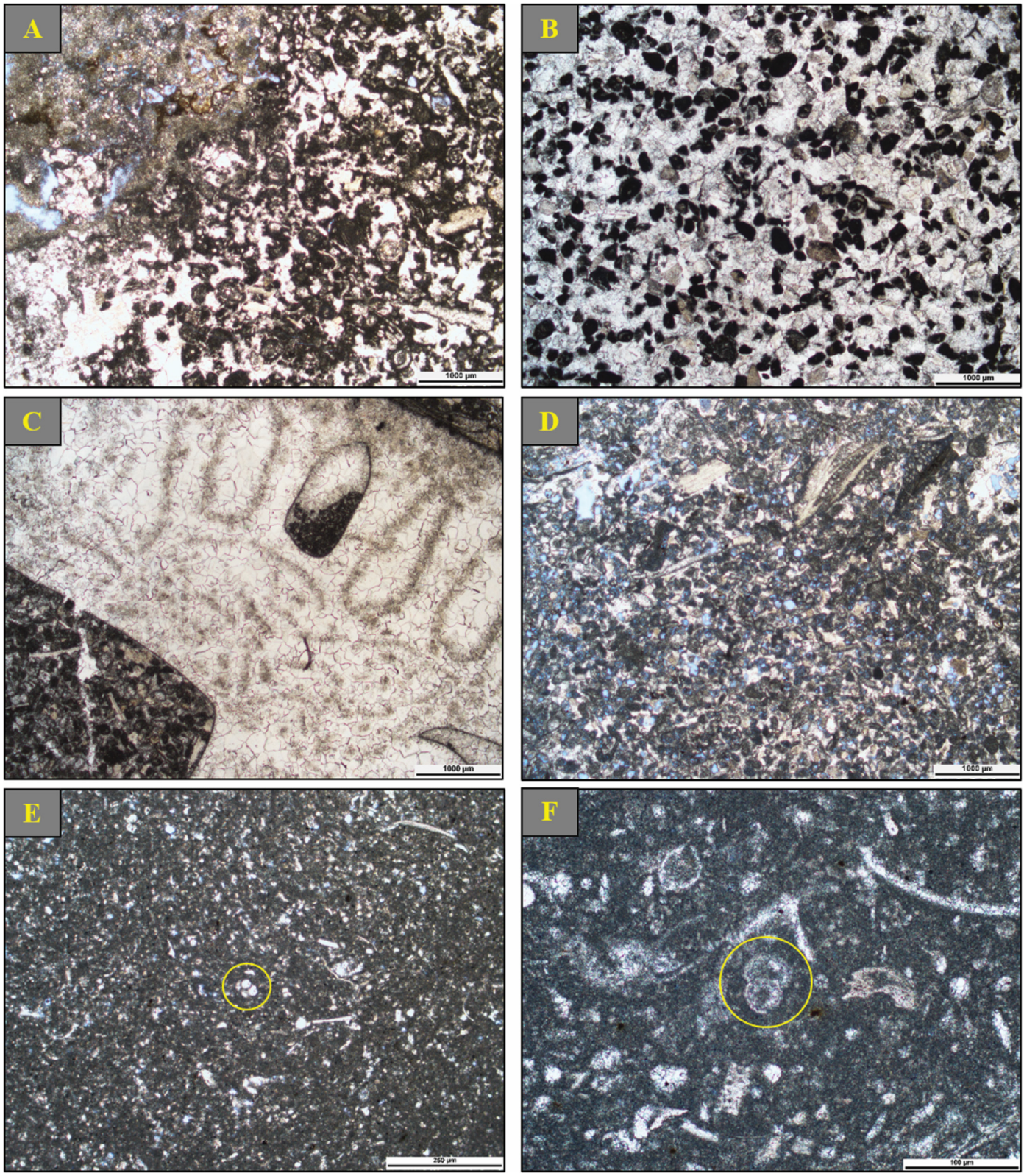

Figure 6. Representative photomicrographs of the high-energy shoal complex facies tract (A–D) and the intrashelf basin facies tract (E–F). Stratigraphic locations of thin sections are shown in Figure 7. (A) Dissolution fabric with a miliolid-echinoid-peloidal mud-dominated packstone. (B) Peloidal-skeletal-caprinid grainstone. (C) Caprinid rudstone with complete blocky calcite cement replacement of aragonite. Note the preservation and geopetal fill of the pallial canal of the caprinid. (D) Peloidal-skeletal grain-dominated packstone with moldic porosity. (E) Spiculitic-foraminiferal mudstone, highlighted in yellow is a four chambered planktonic foraminifera (*Hedbergella*). (F) Foraminiferal-skeletal wackestone with planktonic foraminifera (*Favusella washitaenis*) (yellow circle).

wall structures. The toucasid gastropod packstone can be surrounding larger toucasid rudstones and in the transgressive systems tract passes laterally downdip into skeletal wackestones of the intrashelf basin (Kerans et al., 1995).

Intrashelf Basin Facies Tract

Fine-grained skeletal wackestones and planktonic foramniferal mudstones represent the dominate facies of the intrashelf basin facies tract. High-energy facies of the shoal complex facies tract begins to condense around the Railroad Bridge (Fig. 1). At this location, there is a lateral shift of facies to the recessive weathered thin bedded skeletal wackestones and mudstones. This transition is characterized by the presence of mud-dominated sediments that contain an abundance of planktonic foraminifera. Descriptions of the key lithofacies of the intrashelf basin facies tract are provided below:

Skeletal-Foraminiferal Wackestone (Fig. 6F): Nodular bedded tan to white recessively weathered packages that are bedded to the scale of 10–30 cm. This facies contains an abundance of planktonic or benthic foraminifera, depending on location. There also includes a significant amount of thin-walled *Gryphaea* mollusk fragments. This facies also contains minor amounts of echinoderm and gastropod fragments. The skeletal foraminifera wackestone transitions updip into either mud-dominated subtidal facies or higher energy shoal complexes. Downdip, this facies passes into mudstones.

Spiculitic Planktonic Foraminiferal Mudstone (Fig. 6E): Nodular to slightly bioturbated with abundant planktonic foraminifera, calcispheres, and sponge spicules. Beds are 10–20 cm thick and are dark grey to black in color. This facies transitions updip from skeletal wackestones and the presence of planktonic foraminifera indicates sedimentation in lower energy, basin center environments.

Vertical Facies Successions and Interpretation of Depositional Systems

Facies succession and repetition is an important tool for accurate correlation and interpretation of sequence position in the subsurface (Kerans and Tinker, 1997). Cyclic stacking patterns in greenhouse settings are controlled by very low-amplitude eustatic fluctuations. The result of these low-amplitude changes in sea-level is cycle amalgamation. This impacts stratigraphic resolution in the highstand systems tract (HST) where high-frequency sequences are best defined. This contrast to the transgresstive (TST) where higher resolution cyclicity can be resolved at the cycle scale (Kerans, 2002). A vertical section of the Albian 21 high-frequency sequence at LP4 (Fig. 1) displays a near-ideal vertical facies succession of a wind-dominated foreshore-shoreface complex in the highstand systems tract (Fig. 7). The initial facies of the Albian 21 high-frequency sequence is a massive burrowed peloidal skeletal grain-dominated packstone interpreted to have formed in the lower to upper shoreface. This packstone grades into a cross-stratified skeletal grain-dominated packstone that was deposited in the upper shoreface. Above this unit is a caprinid rudstone with fragments of coarse rudist debris indicating a sedimentation style that is consistent with a plunge-zone environment within the upper shoreface. The coarse rudist rudstone is overlain by caprinid skeletal grainstones that display trough cross-stratification characteristic of the upper shoreface (Fig. 7). The final lithofacies assemblage is a peloid caprinid skeletal grainstone with seaward dipping accretionary stratification indicative of a foreshore complex. This stacked section is capped by a brief period of exposure, with karst dissolution textures and dissolution pits on the order of 10–30 cm as supporting evidence.

Low-amplitude sea-level fluctuations have a major effect on cycle development and vertical stacking patterns in this ramp system. The low dip angle of the depositional profile promotes the lateral shifting of facies, rather than complete vertical trends (Kerans, 2007). This contrasts with the well-defined vertical stacking patterns observed in carbonate ramp systems developed during transitional greenhouse-icehouse regimes, as shown by outcrop studies of the San Andres Formation in the Guadalupe Mountains by Kerans and Fitchen (1995) along the Algerita Escarpment, New Mexico, and by Sonnenfeld and Cross (1993) in Last Chance Canyon, New Mexico.

Depositional Models

The depositional history of the late Albian Maverick intrashelf basin has been described in two systems tract specific depositional models (Fig.8) because of the facies partitioning that exist (Kerans et al., 1995). The depositional model for both the TST and HST ramp systems can be subdivided into the inner, middle, ramp crest, and outer ramp environments (Burchette and Wright, 1992; Kerans and Fitchen, 1995). The TST depositional model consists of mud-dominated subtidal facies with well-developed (1–5 m thick) pancake-shaped radiolitid-chondrodont buildups. In this study, the buildups are biostromes that are dominated by toucasid rudstones that develop in outer shelf environments, as observed at Nine-Mile Bend (LP1) and Deadman's Canyon (LP2). Variations in the depositional style of the HST model is most marked at the ramp crest of each high-frequency sequences. HST deposits along the northern margin of the Maverick intrashelf basin can be interpreted as either wave-dominated or tide-dominated environments. Through detailed lateral facies mapping, Kerans (2007) showed that the grainstones of the Albian 19 high-frequency sequence form as the result of a lagoon-inlet-barrier complex. The evidence for this is observed at Painted Canyon (Fig. 1) where paleocurrent data indicate a bimodal north-south (basinward) exchange of flow and a lower set of sigmoids that have depositional dips that build to the west, perpendicular to the ramp crest (Kerans, 2007). By contrast, in this investigation, the ramp crest of the Albian 21 high-frequency sequence is interpreted as a wave-dominated system with well-developed laterally accreting foreshore and shoreface grainstones.

STRATAL GEOMETRIES AND FACIES PATTERNS

Using control data from the five measured sections (LP1–LP5) located in a dip-oriented transect (Fig. 1), as well as previous sections of Kerans et al (1995) and Kerans (2002), 3D surfaces were traced across a digital outcrop model for the Lower Pecos River canyon (Fig. 9). Using facies data from the measured sections and the dip angles interpreted from the 3D modeled surfaces a projected dip-oriented cross-section was created. This high-resolution cross-section highlights the lateral facies transitions relative to the sequence stratigraphic framework (Fig. 10). The interpretation and distribution of facies within the sequence stratigraphic framework will be discussed in terms of an updip area from Nine-Mile Bend to Deadmans Canyon, a transitional area at the railroad bridge, and the intrashelf basin area at the Highway 90 Bridge (Fig. 1).

Updip Area (Nine-Mile Bend–Deadmans Canyon)

The Nine-Mile Bend measured section (LP1) represents the most updip section of this study, the section as measured is 110 m thick, and includes the Albian 18–22 high-frequency sequences. It contains the thickest section (53 m) of the Albian 19 and 20 high-frequency sequences observed on the Lower Pecos River. The most striking component of the updip section is the development of a major peloidal skeletal grainstone in the Albian 21 high-frequency sequence that expands within a short distance

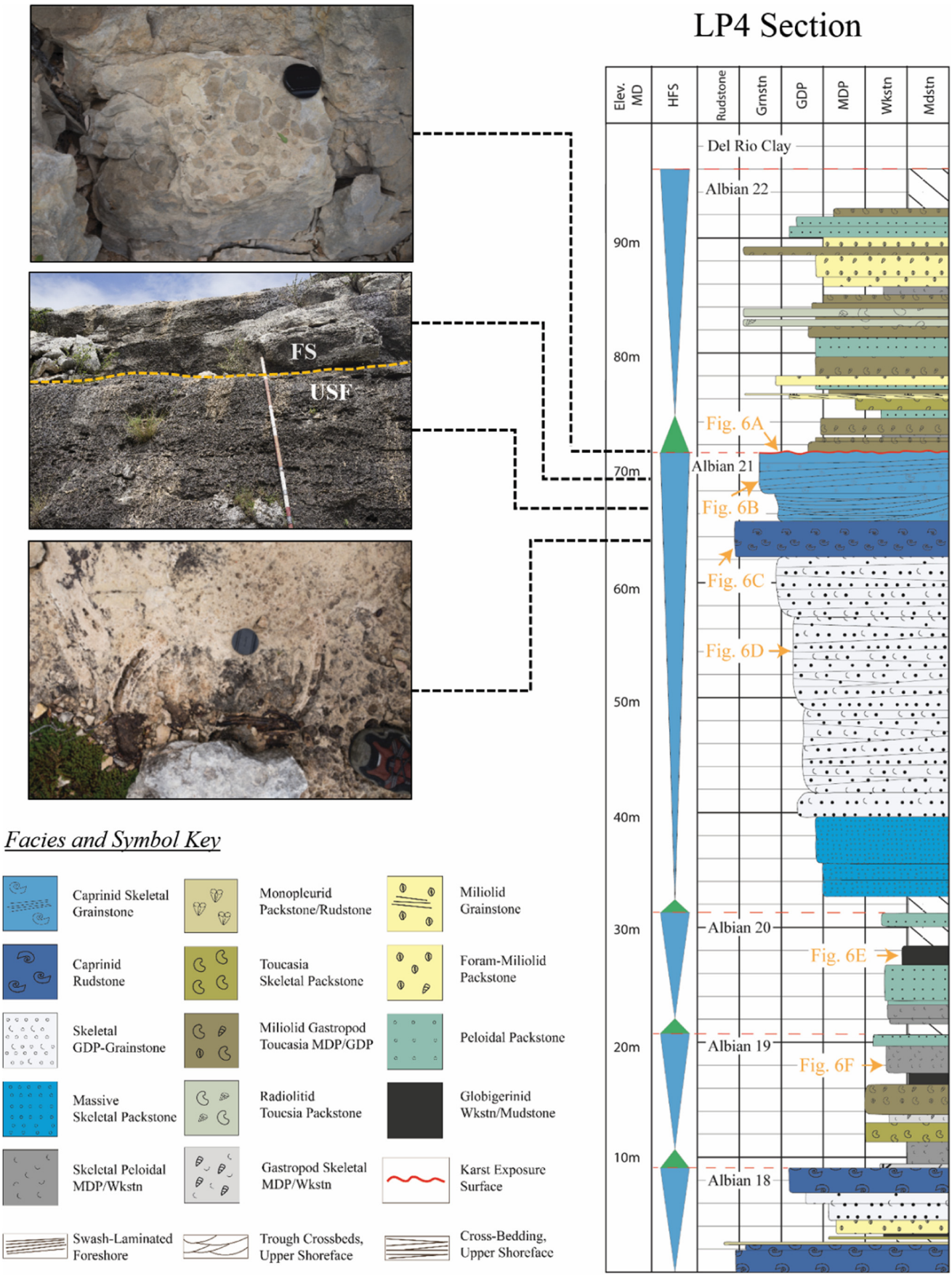

Figure 7. Measured section LP4, demonstrating the condensed sections of the Albian 19 and 20 high-frequency sequences and a near-ideal stacking pattern of a foreshore-shoreface complex formed within the highstand systems tract of the Albian 21 high-frequency sequence. Outcrop photos show transition from caprinid rudstone, upper shoreface trough cross-beds, laterally accreting swash laminated foreshore complex, and karst dissolution pit at the Albian 21 upper sequence boundary.

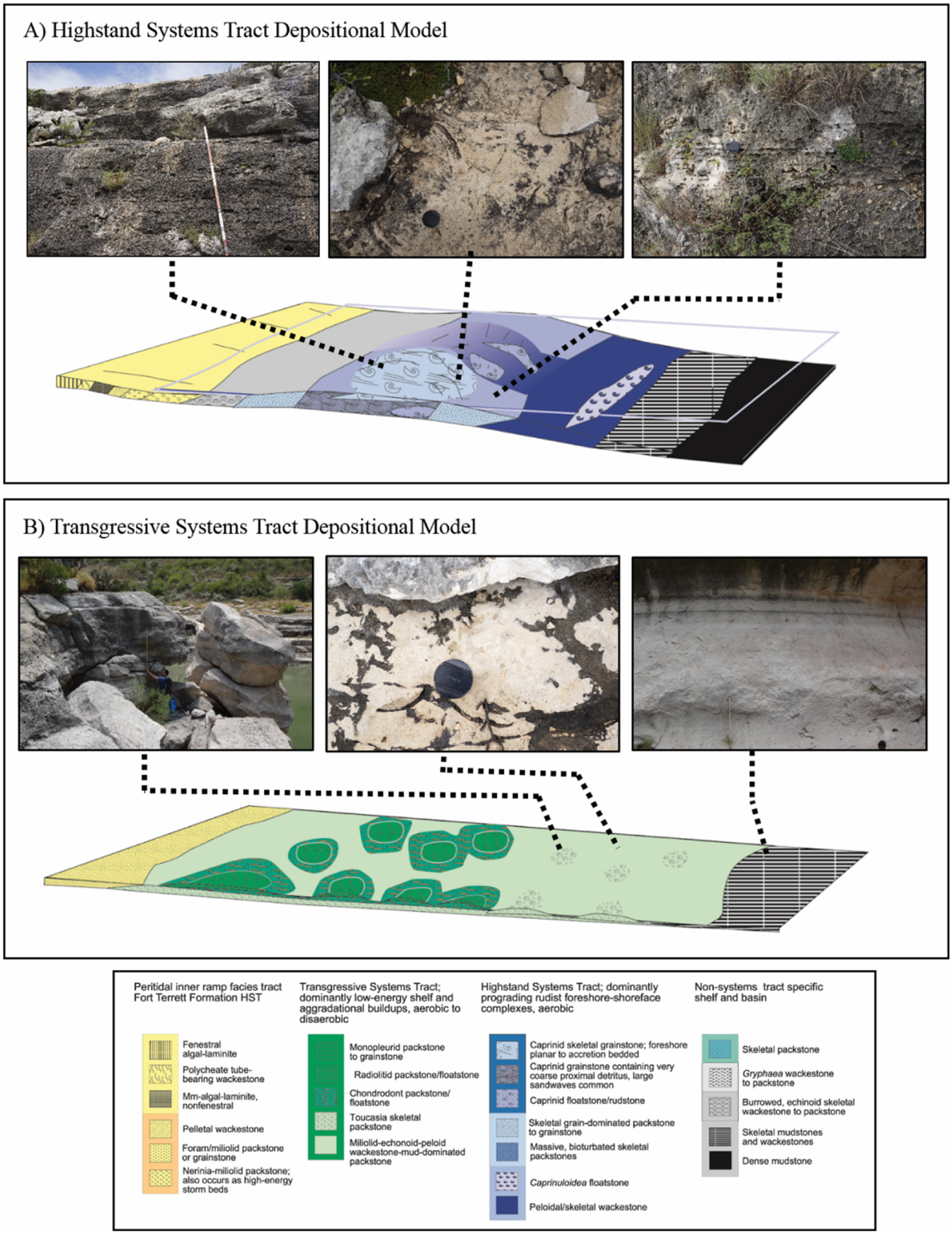

Figure 8. Depositional model for the late Albian high-frequency sequences (Kerans, 2002). (A) Highstand systems tract (HST) model, including both the wave-dominated foreshore-shoreface model and the tide-dominated tidal inlet model. (B) Transgressive systems tract (TST) model showing outer ramp toucasiid biostromes that pass basinward into skeletal wackestones. Outcrop photos are provided for key elements of the depostional models. Modified after Kerans (2002).

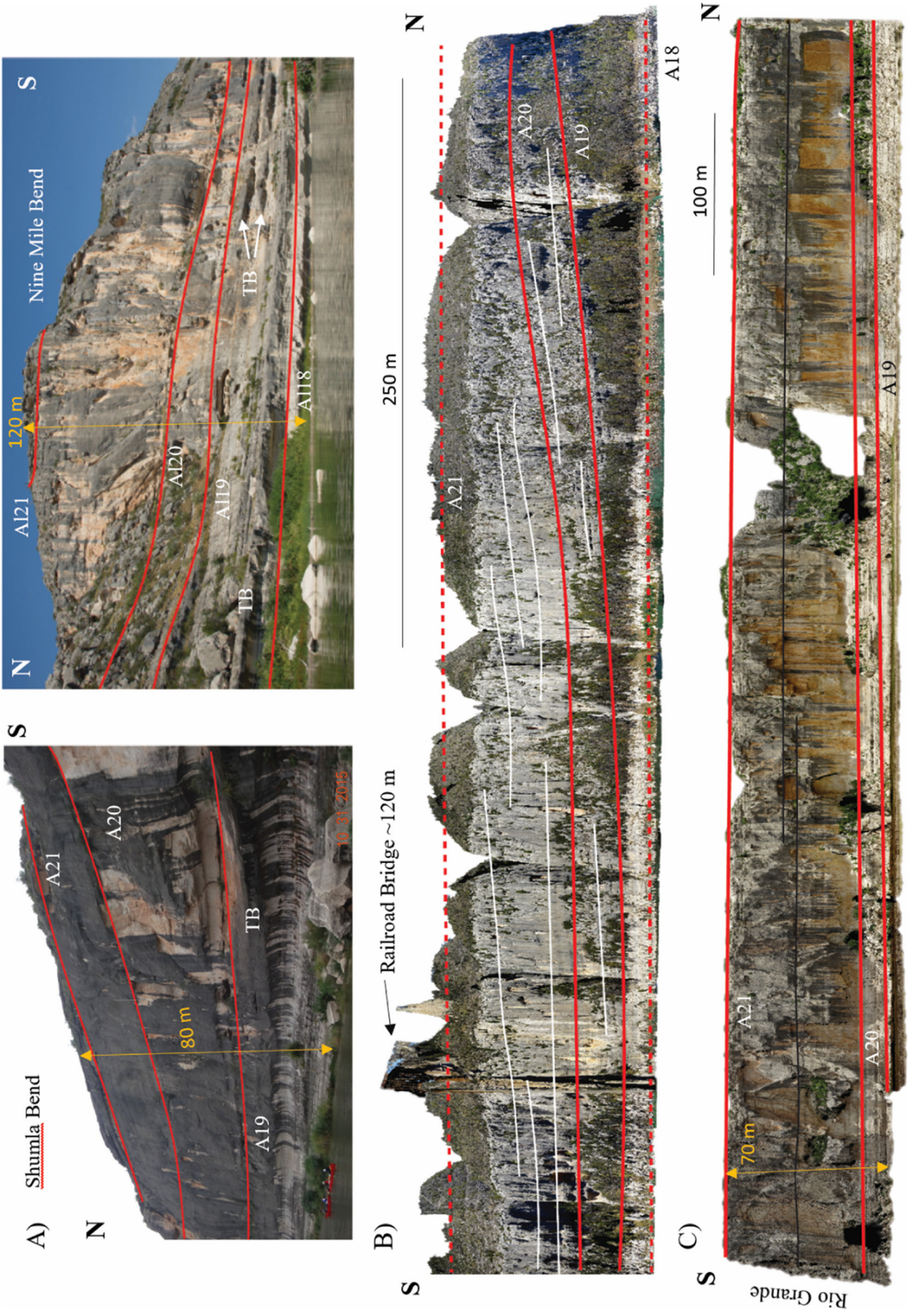

Figure 9. Interpretation of the Albian high-frequency sequence from photographs and the digital outcrop model. (A) Shumla Bend–Nine-Mile Bend, showing the initial development of the Albian 21 high-frequency sequence; note the multiple levels of toucasid biostromes (TB) in the Albian 19 high-frequency sequence. (B) Panel from the DOM at 10x vertical exaggeration showing the downlap of the Albian 19 and 20 high-frequency sequences; note that dip angles are on the order of 0.4°. (C) Panel from the DOM at 2x vertical exaggeration, demonstrating the condensed intrashelf basin facies of the Albian 19 and 20 high-frequency sequences, and the thick prograding grainstone of the Albian 21 high-frequency sequence.

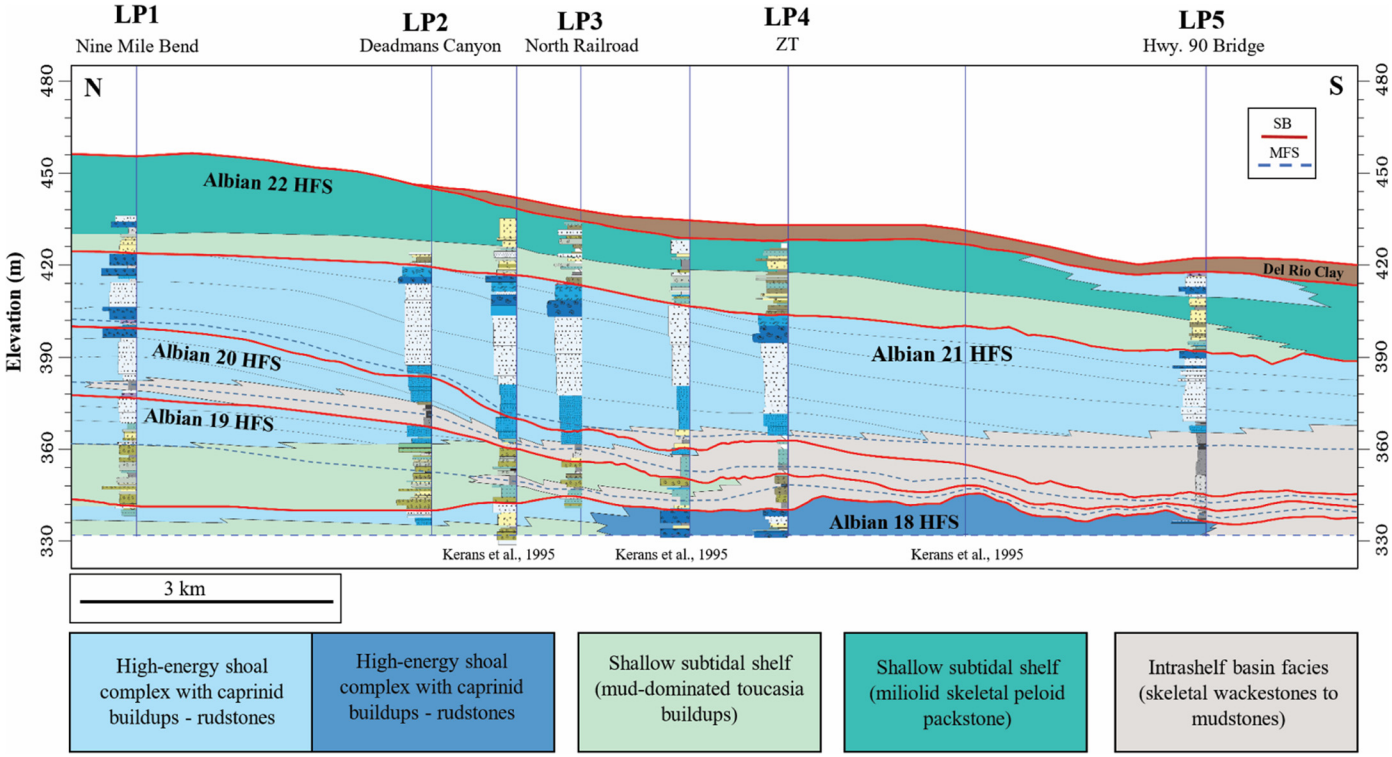

Figure 10. High-resolution sequence stratigraphic framework for the Lower Pecos River. Sequence boundaries (in red) were mapped from the digital outcrop model and facies tract distributions were correlated within these boundaries using the stratigraphic measured sections. SB, sequence boundary; MFS, maximum flooding surface.

along dip (200 m) and can be traced from an approximately 10 m thick section at Shumla Bend to a 25 m thick section at the Nine-Mile Bend section (LP1) (Fig. 9A); it thickens to 35 m at the LP2 section. The facies assemblages observed in the updip section contain an initial skeletal-peloidal packstone that deepens into toucasid biostromes. There are three well-developed intervals of the toucasid rudstone facies with a thickness of 2–3 m that are capped by bedded gastropod miliolid packstones at the LP1 section. The initial skeletal packstone is interpreted to be shallow water facies that marks the top of the Albian 18 high-frequency sequence, and the deepening into toucasid rudstone (mud-dominated shallow subtidal) facies represent the transgressive systems tract of the Albian 19 high-frequency sequence. The toucasid mounds shallow into caprinid-skeletal packstones that are prograding over the lower energy buildups. This shallowing event and shift to higher energy is interpreted to be the highstand portion of the Albian 19 high-frequency sequence. The HST portion of the Albian 19 significantly thins (12 m) over 1 km in dip-distance from Painted Canyon (Kerans et al, 1995) (Fig. 1).

At Deadmans Canyon (LP2), the measured section is 90 m thick, and includes the Albian 18–21 high-frequency sequences. At the base there is a sharp contact with a 1 m caprotinid mud-dominated packstone/rudstone that has evidence of local microkarst development along the same contact updip (Kerans, 2007). The caprotinid rudstone is then followed by an 18 m thick cross-bedded peloidal skeletal grainstone that is capped by a 3 m thick caprinid rudstone. Above this contact there is a 1 m thick caprotinid rudstone (indicated deepening) that is followed by a 35 m thick cross-bedded peloidal skeletal grainstone with the upper 5 m consisting of caprinid rudstones and swash-laminated caprinid skeletal grainstones. The development of the local microkarst below the first caprotinid rudstone is interpreted as a period of brief exposure and the top of the Albian 18 high-frequency sequence. The Albian 20 high-frequency sequence is missing a significant TST–dominated facies assemblages and the initial floodback is marked by a subtidal caprotinid rudstone and thin skeletal wackestone. The 18 m peloid skeletal grainstone that shallows and progrades over the caprotinid rudstone is interpreted as the HST of the Albian 20 high-frequency sequence. The major cliff former of the 35 m peloid skeletal packstone with caprinid rudstones is interpreted as the forced regressive HST of the Albian 21 high-frequency sequence. Overall, the sedimentation patterns observed in the updip section, at Nine-Mile Bend and Deadmans Canyon, represent a high-energy grain-dominated system, as compared with sections to the south.

Transitional Area (Railroad Bridge)

In the area around the Pecos River Railroad Bridge (LP3 and LP4), the grain-dominated units observed in the updip section begin to shift laterally into skeletal wackestones/ mudstones of the intrashelf basin. The transitional section as measured in LP3 and LP4 is a total of 96 m thick and includes the Albian 18–22 high-frequency sequences. The key observation in this part of the canyon is the 18 m thin-bedded package of intrashelf basin facies that the equivalent of the 50 m thick rudist-dominated assemblages 7.5 km updip at Painted Canyon (Kerans et al., 1995). The downlap and condensation of the Albian 19 and 20 high-frequency sequence sections can be traced downdip from Deadmans Canyon past the Railroad Bridge (Fig. 9B). The facies assemblages documented at LP4 consist of an 8 m thick package with two levels of caprinid rudist buildups on the scale of 3 m. The lower buildup of caprinid rudstones is capped by a 20 cm monopleurid rudstone. These caprinid rudstone buildups are directly overlain by an 18 m thick unit of recessively weathered, slope-forming beds that contain facies dominated by peloidal toucasid mud-dominated packstones/wackestones, skeletal-foraminiferal wackestones, and spiculitic-foraminiferal mudstones. The shallow-water, high-energy caprinid rudists are interpreted to represent the highstand systems tract of the Albian 18

high-frequency sequence. The condensed section of 18 m thick intrashelf basin facies represents the entire deposition of the Albian 19 and 20 high-frequency sequences. The condensed section passes upward into the previously described 42 m thick vertical succession of A21 age (Fig. 7) that consists of burrowed massive peloidal grain-dominated packstones to cross-stratified peloidal skeletal packstone/grainstones. The A21 vertical succession is interpreted to represent high-energy ramp crest facies that were deposited in a wave-dominated foreshore-shoreface environment. This forced regressive interval represents the highstand of the Albian 21 high-frequency sequence and downlaps over the condensed sections of the Albian 19 and 20 high-frequency sequences. The karst exposure surface at the top of this interval is the Albian 21 sequence boundary, which separates the prograding Albian 21 high-frequency sequence from the backstepping toucasid-miliolid packstone dominated facies of Albian 22 high-frequency sequence.

Intrashelf Basin Area (Highway 90 Bridge)

In the southernmost area of this study, at the confluence of the Lower Pecos River and the Rio Grande, the Highway 90 measured section (LP5) is a total of 80 m thick and includes the Albian 18–22 high-frequency sequences. The most impressive observation here is the increasing proportion of intrashelf basin facies and the major cliff former that consist of a 42 m thick unit of skeletal peloid packstone/grainstones. There is a small exposure of caprinid rudstone at the base of the Highway 90 Bridge, inferred to represent the top of the A18 sequence. This caprinid facies assemblage is directly overlain by 10 m of intrashelf basin deposits, composed of peloidal mud-dominated packstones, skeletal wackestones, and foraminiferal mudstones that are indicative of deposition in deeper water conditions during A19 and A20 deposition. The condensed section is overlain by a 20 m package of massive peloidal skeletal wackestones and packstones that transition upward into 22 m of cross-stratified skeletal grain-dominated packstones. Near the top of this sequence there is a 2 m thick reworked caprinid fragment rudstone. This sequence is interpreted to represent shallow-water foreshore-shoreface environments of the prograding Albian 21 high-frequency sequence. At the upper sequence boundary of the Albian 21 high-frequency sequence, there is evidence of exposure and heavily micritized grains that are similar to the foreshore complex documented updip at the LP4 section. The 42 m thick package of skeletal packstones/grainstones is overlain by a 24 m mixed succession of caprotinid/caprinid rudstones, miliolid gastropod packstones, gastropod toucasid packstone/rudstone, and peloidal skeletal packstone/wackestone. This retrogradational interval is interpreted to represent the backstepping Albian 22 high-frequency sequence. The sequence boundary at the top of the Albian 22 high-frequency sequence is a bored firmground that is most likely marine in origin (Kerans et al., 1995), and is unconformably overlain by the Cenomanian Del Rio Clay and Buda Limestone.

3D Stratigraphic Model

The 3D stratigraphic model was intended to faithfully characterize the stratal geometries of the Albian 18–21 high-frequency sequences. Construction of the model integrated data interpreted from the digital outcrop model and the five sections that were measured along the Lower Pecos River. The study also mapped the top of the Albian 22 high-frequency sequence (top of Devils River) from NAIP 2 ft aerial imagery and extracted elevation values from the U.S. Geological Survey 10 m National Elevation Dataset. The Albian 22 high-frequency sequence was then gridded over a 40 sq. km area of the Lower Pecos River, and corrections were applied to the DOM using control points. The Albian 22 high-frequency sequence surface was used to guide the gridding of the surfaces using top-down conformance relationships for the Albian 18–21 high-frequency sequences extrapolated from the canyon-derived interpretations. The dip angles of the ramp profile were then extracted from structure contour maps created for each of the high-frequency sequence, using similar surface attribute extraction methods to those used in subsurface datasets. The Albian 18 high-frequency sequence is a flat surface with dips averaging 0.08° however locally higher dips in areas with a higher concentration of rudist mounds. The change in stratal geometry of the Albian 19–20 high-frequency sequences correlates with lateral shift in facies from grain-dominated facies on the ramp crest into mud-dominated intrashelf basin deposits (Fig. 11). The Albian 19 high-frequency sequence has an average dip angle of 0.2° with a bimodal distribution of dip angles that indicates the shelf-to-basin transition. The dip angles over this transition decrease from 0.4° on the ramp crest to dip angles of 0.15° in the intrashelf basin. The Albian 20 high-frequency sequence depositional profile is at a higher angle than the top of the Albian 19 high-frequency sequence and has average dips of 0.3°. A bimodal distribution of dip angles is also observed in the Albian 20 high-frequency sequence with ramp dip angles at 0.6° and an intrashelf basin angles of 0.2°. The dip-angle histogram for the Albian 21 high-frequency sequence ramp morphology shows a unimodal distribution of angles that average 0.33°. The unimodal distribution of dips within the Albian 21 high-frequency sequence indicates that the shelf-to-basin transition occurs approximately 20 km basinward of this investigation. The interpretation of the shelf-to-basin transition can be shown on the modeled structure contour maps along with a comparison of dip angle, dip width, and progradation/aggradation ratios (Fig. 12).

DISCUSSION

This study suggests that the origin of the late Albian Maverick intrashelf basin resulted from subtle topographic expression (1–3 m) (Fig. 10) that contributed to the divergence of sediment accumulation rates within the carbonate factory. This model of intrashelf basin evolution is similar to that proposed for the Bab intrashelf basin and the intrashelf basin development with the Savark-Naith formations (Droste, 2010; Razin et al., 2010; Van Buchem et al., 2002a). Through detailed sequence stratigraphic analysis it can be demonstrated that eustatic fluctuations and accommodation are the most important factors that control the depositional profile of intrashelf basin ramp systems (Razin et al., 2010; Van Buchem et al., 2002a). While the drivers and dynamics for the evolution of intrashelf basins are well-documented, there is still a lack of understanding of the primary controls on the origin and location of intrashelf basin systems.

Evolution of the Northern Margin of the Late Albian Maverick Intrashelf Basin

The evolution of the late Albian Maverick intrashelf basin can be characterized in four main stages as demonstrated in Figure 13. The first stage of evolution is represented by the Albian 18 TST, where the rate of sediment accumulation is considered to be equal across the platform top. In the HST stage of the Albian 18 high-frequency sequence the initial development of caprinid rudist buildups provides the earliest evidence of topographic expression (1–3 m) for the Maverick intrashelf basin. This early relief is topographically flat, but dominated by subtle buildups. The second stage of evolution (Albian 19–20 high-frequency sequences), is characterized by rapid aggregation of the ramp margins, and create the major differentiation between the margin and intrashelf basin. The deposits across the ramp margin consist of facies assemblages that are dominated by radiolitid-condrodontid-toucasiid rudist buildup in the transgressive system tracts and caprinid grainstone-rudstones in the highstand system tracts. The third stage of evolution (Albian 21 high-frequency sequence), consists of a major progradational wedge that down-

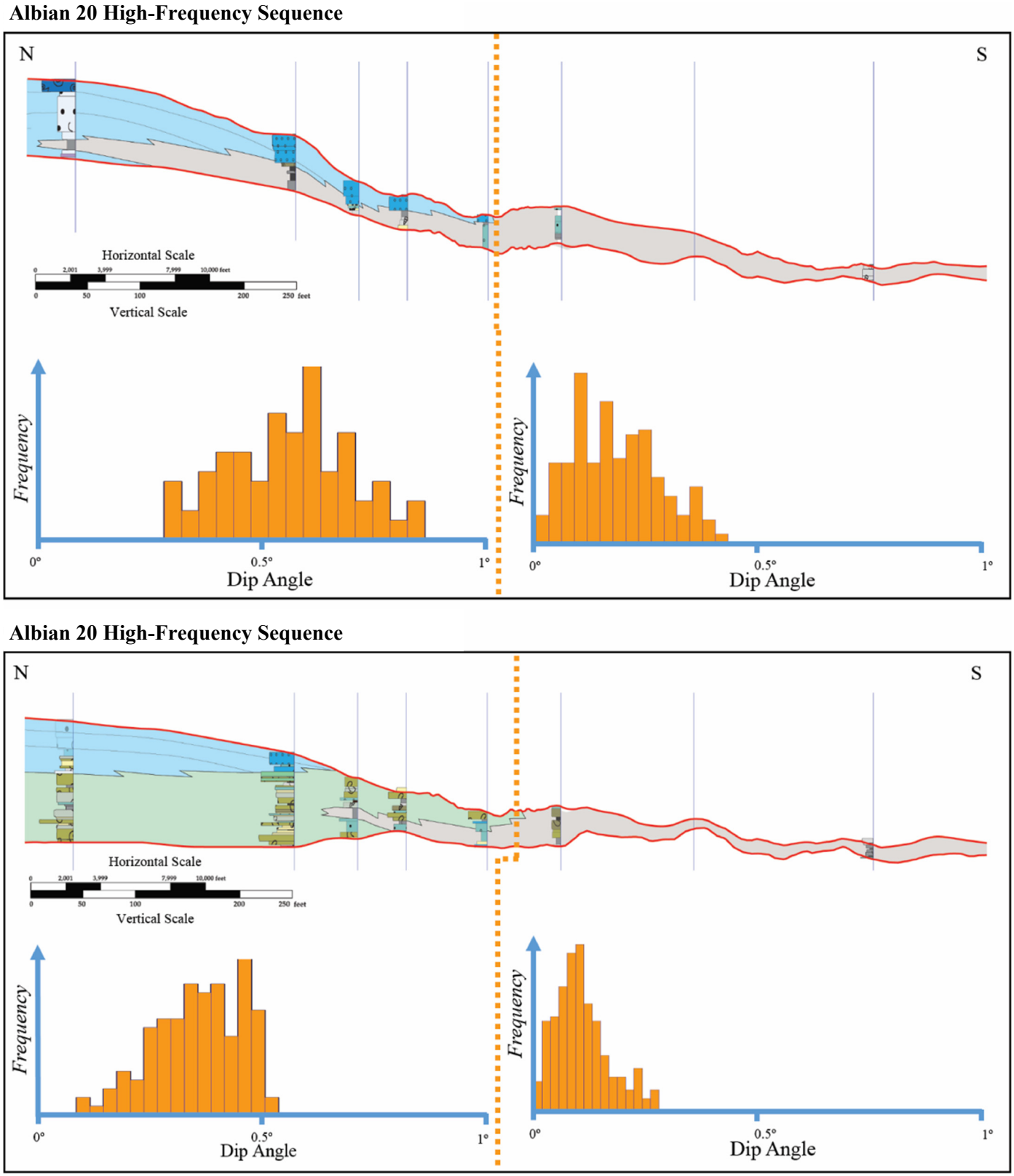

Figure 11. Relationship of lateral facies transitions to changes in dip angle of the depositional profile for the Albian 19 and 20 high-frequency sequences. As the dip of the depositional profile increases, sedimentation transitions from higher energy grain-dominated assemblages into mud-dominated facies of the intrashelf basin.

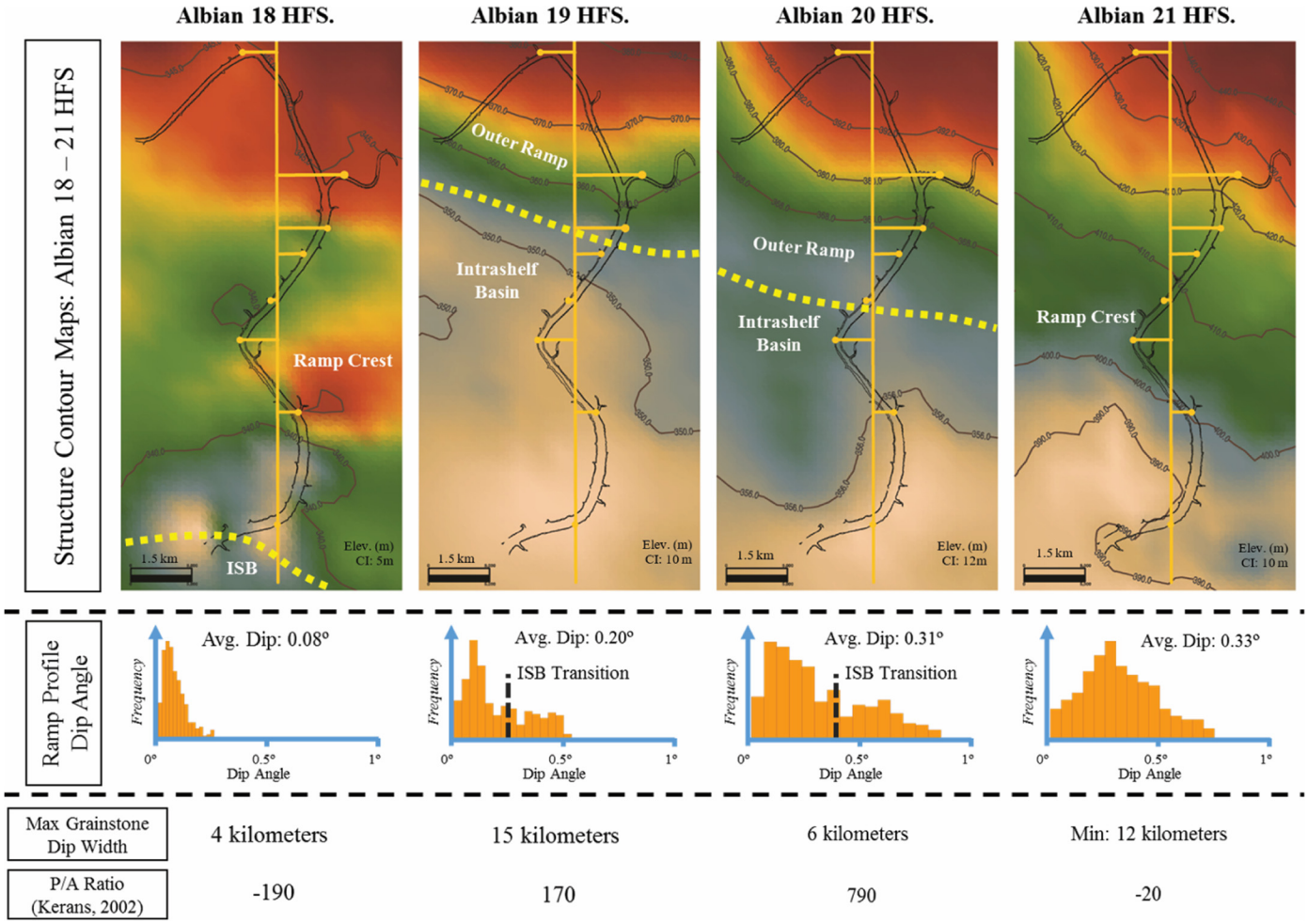

Figure 12. Structure contour maps with the shelf-to-basin transition defined by structural positioning and facies observation in outcrop. The orange N–S line highlights the cross-section in Figure 10. The location of measured sections are shown by orange dots along the Pecos River (outlined in black). Comparisons of dip angle, dip width, and progradation/aggradation (P/A) ratios are made for each of the high-frequency sequences (HFS). Note that the Albian 21 high-frequency sequence ramp crest is situated over the condensed transition of the Albian 19 and 20 high-frequency sequences. The Albian 21 high-frequency sequence shelf-to-basin transition lies approximately 20 km basinward of this study area.

laps and infills over the Albian 19 and 20 high-frequency sequences. The fourth and final stage of Maverick intrashelf basin deposition is characterized by the backstepping deposits of the Albian 22 and 23 high-frequency sequence.

Controls on Origin and Evolution of Intrashelf Basin Systems

The origin of intrashelf basins is thought to result from small differences in topography that results in the development of differential rates of sedimentation (Van Buchem et al., 2002a). The creation of minor topographic expression is enough to trigger the formation of intrashelf basin deposits during times of relative sea-level rise (Razin et al., 2010). The differential topography can result from antecedent topography, differential subsidence, tectonic influence, or the construction of subtle mound geometries. In the case of the Maverick intrashelf basin, the likely driver behind the initial positive topographic expressions is the development of caprinid rudist mounds that develop after the major maximum flooding event of the Albian 6 CS (Albian 18 MFS) and within the HST of the Albian 18 high-frequency sequence. The rudist complex in the Albian 18 high-frequency sequence spans 4 km in dip width and bedding is characterized by large-scale swales-hummocks that develop on the order of 1–3 m.

Another possible explanation for the origin of intrashelf basin systems could be ecoeustatic drivers that cause the carbonate factory to shut down, leading to broad areas of subdued sedimentation rates. During the Cretaceous, there was a tendency for ocean circulation to become stagnant and result in the stratification of temperature, salinity and oxygen content within the water column (Meyer and Kump, 2008). Several ocean anoxic events (OAE) are recognized across the Comanche Platform, with well-constrained and documented evidence for the major Aptian OAE 1b and Cenomanian-Turonian OAE 2 events (Phelps et al., 2014). The exact stratigraphic location of the OAE 1d event on the Comanche shelf is not well-constrained, but recent studies have placed the event in the late Albian. (Phelps et al., 2015). It is possible that stress on the carbonate factory from OAE 1d contributed to the evolution of the .

The primary driver of intrashelf basin evolution is accommodation through its control on the morphology of the ramp profile (Razin et al., 2010). The dip angle of the depositional profile influences sedimentation by controlling the energy of the system. Lower angle profiles result in energy regimes that are lower, such that sedimentation results in mud-dominated facies assemblages

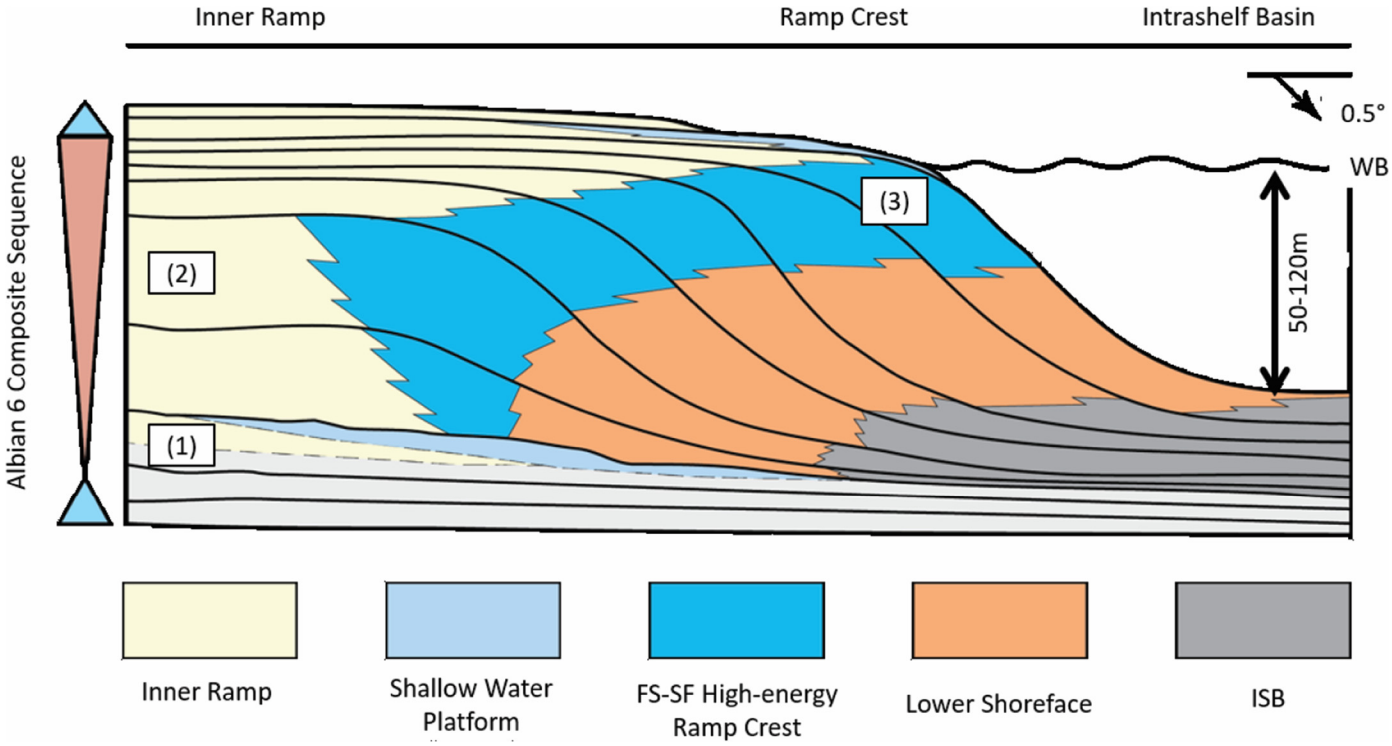

Figure 13. Idealized sequence stratigraphic evolution for the Maverick intrashelf basin. This idealized model highlights the key stages of intrashelf basin development. (1) aggradation of the platform top and development of initial topographic expression, (2) aggradation and formation of the intrashelf basin shelf-margin, (3) progradation and infill into the basin, and (4) final back-step onto the intrashelf basin margin (Kerans, 2002; Razin, 2010).

typical of intrashelf basin deposits. By contrast, higher angle profiles promote higher-energy systems that result in grain-dominated facies assemblages (Droste and Van Steenwinkel, 2004; Razin et al., 2010). There is also a connection between carbonate sediment type and the ramp angle; increasing the dip angles results in a shift from formniferal skeletal wackestones and foraminiferal mudstones into rudist-bearing, bioclastic grain-dominated assemblages. Average dips across the ramp profile also have an impact on the lateral distribution of high-energy grainstones. This is demonstrated by the Albian 19 high-frequency ntrashelf basin sequence has lower average dip angles across the profile, when Albian 19 high-frequency sequence. However, the grainstone dip-width of the Albian 19 high-frequency sequence is 9 km wider then compared to the higher angle Albian 20 high-frequency sequence.

Dip Angle of the Depositional Profile and Facies Variability

Accommodation and energy are the fundamental controls on the dip angle of the depositional profile, and is the key influence on depositional patterns observed on carbonate ramp systems that transition into intrashelf basin deposits. Increases in depositional dip angles promotes an increase in energy and drives sedimentation at the ramp crest. With the proper accommodation, aggradation of the margin can result and develop a clear transition from grain-dominated system to a low-energy mud-dominated (Droste and Van Steenwinkel, 2004; Razin et al., 2010). This increase in energy leads to higher sedimentation rates and continues to build the ramp margin of intrashelf basin systems through aggradation. The increase in energy that results from an increase in fetch of the basin system, combined with an appropriate ramp morphology, promotes the exchange of tidal currents which leads to deposition of facies in a lagoon-inlet-barrier complex as documented in the lower angle (0.2°) HST of the Albian 19 high-frequency sequence. In similar HST settings of the Albian 20 and 21 high-frequency sequences greater dip angles (0.3°) promote a higher-energy wave-dominated environment that leads to the deposition of deposits within a foreshore-shoreface complex.

Similar relationships between stratal geometries and facies have been documented in the Natih 'E' Formation (Droste, 2010; Droste and Van Steenwinkel, 2004) and the Shuaiba Formation (Van Buchem et al., 2002a). Dip angles across the margin of intrashelf basins can range from less than 0.5° and up to 35°. The deposition of steeper angle clinoforms along the intrashelf basin margin have been attributed to a contrast between high-stand versus lowstand development (Droste and Van Steenwinkel, 2004). However, lowstand wedges are not observed in the Maverick intrashelf basin. Instead, the depositional profile of the Maverick intrashelf basin is less than 1° throughout the entire evolution of the system. These relationship observed between changes in dip angles and facies distributions are directly analogous to the Bab intrashelf basin of the Shuaiba Formation, where dips range from lower energy deposits with 0.1° to higher-energy deposits with 5° dip angles (Droste, 2010; van Buchem et al., 1996). It is also important to note that while the morphology of the ramp profile along the northern margin of the Maverick intrashelf basin never exceeds 1°, there is variability along the margin. There have been documented dip angles that reach 20° on the western margin of the Maverick intrashelf basin in Mexico (Osleger et al., 2004). This increase in dip angle of the depositional profile occurs there as a function of greater accommodation and much higher energy regimes along that portion of the ramp margin.

CONCLUSION

Documenting the shelf-to-basin transition of the late Albian Maverick intrashelf basin provides an analog for unraveling the stratigraphic complexity with vertical and horizontal resolution

that is higher than any subsurface dataset. Understanding the shelf-to-basin transition of intrashelf basin systems has important implications at the reservoir scale. Knowing the distribution/variability between highstand grainstone facies to intrashelf basin deposits and the relationship to the geomorphic expression at the shelf to intrashelf basin transition will help improve reservoir understanding of intrashelf basin petroleum systems.

Interpretation of a high-resolution digital outcrop model and vertical measured sections show that lateral facies transitions of grain-dominated facies into skeletal wackestones/glogbigerinid mudstones occurs across a decrease in the depositional slope angle by at least 25 percent for the Albian 19 and 20 high-frequency sequences. The condensed section that represent the transition into intrashelf basin facies of the Albian 19 and 20 high-frequency sequences occurs 7.5–8 km downdip from the ramp crest. Documentation of Albian 19 and 20 high-frequency sequences along the Lower Pecos River confirms the relationship between the dip angle of the slope and lateral transition of facies across the depositional profile. Higher-angle dips of the slope profile promotes winnowing and preservation of grain-dominated facies assemblages found along the intrashelf basin margins and the decrease in slope angle marks the transition to mud-dominated intrashelf basin facies with lower-angle dip profiles. The forced regressive Albian 21 high-frequency sequence that represents the infills stage of intrashelf basin evolution fills the available accommodation space created by aggradation of the intrashelf basin margins, and with a slope profile of 0.33° has the greatest depositional dips documented along the margin of the intrashelf basin.

The depositional models developed for the highstand and transgressive systems tract for the Maverick intrashelf basin ramp system by Kerans (2002) accurately characterizes lateral facies changes observed on the Lower Pecos River. The highstand wave-dominated foreshore-shoreface model is represented in an ideal facies succession at the ramp crest of Albian 21 high-frequency sequence. The highstand of the Albian 18 high-frequency sequence demonstrates the first evidence of positive topographic expression that helps drive the separation of sedimentation rates that leads to the development of an intrashelf basin system. The Albian 19 high-frequency sequence grainstones have a dip width of 15 km with average depositional profile of 0.2° and aggradationally stack to form the ramp margin of the Maverick intrashelf basin. The Albian 20 high-frequency sequence have a greater averages depositional dip of 0.3° with shorter, 6 km dip-widths of HST grainstones. The Albian 21 high-frequency sequence is a forced regressive progragrading wedge that steps basinward nearly 30 km. The minimum dip width of the Albian 21 high-frequency sequence is 12 km with a depositional profile that averages 0.33°.

A key observation of this study is the comparison between similar constructional differential-accumulation driven intrashelf basins. The Maverick intrashelf basin has an origin and evolution that is comparable to documented intrashelf basins in the Middle East. The observations of the Maverick intrashelf basin supports the constructional differential-accumulation model. This is important because it highlights the ability of the carbonate factory to develop a topographic response to eustatic fluctuations and the control that accommodation exhibits on the evolution of these systems through subtle changes in depositional slope angles. The constructional development of the Maverick intrashelf basin also provides insight to the processes that formed the Fort Stockton and East Texas intrashelf basin systems.

ACKNOWLEDGMENTS

Funding for this research was graciously provided by the Reservoir Characterization Research Laboratory (RCRL), an Industrial Associates program at the Bureau of Economic Geology at the University of Texas at Austin. We thank Kris Voorhees and Benjamin Smith for their assistance in the field and for the countless discussions on carbonate systems. Bob Loucks and Lowell Waite provided helpful reviews on early drafts of this manuscript. Detailed and well-thought out reviews by Tom Ewing, David Hull, and Andrea Nolting significantly improved the quality of the final manuscript.

REFERENCES CITED

Alsharhan, A., 1985, Depositional environment, reservoir units evolution, and hydrocarbon habitat of Shuaiba Formation, Lower Cretaceous, Abu Dhabi, United Arab Emirates: American Association of Petroleum Geologists Bulletin, v. 69, p. 899–912.

Alsharhan, A., 1995, Facies variation, diagenesis, and exploration potential of the Cretaceous rudist-bearing carbonates of the Arabian Gulf: American Association of Petroleum Geologists Bulletin, v. 79, p. 531–550.

Bebout, D. G., and R. G. Loucks, 1983, Lower Cretaceous reefs, South Texas, *in* P. A. Scholle and others, eds., Carbonate depositional environments: American Association of Petroleum Geologists Memoir 33, Tulsa, Oklahoma, p. 441–444.

Bellian, J. A., C. Kerans, and D. C. Jennette, 2005, Digital outcrop models: Applications of terrestrial scanning lidar technology in stratigraphic modeling: Journal of Sedimentary Research, v. 75, p. 166–176, <http://doi.org/10.2110/jsr.2005.013>.

Bourget, J., R. Nanson, R. B. Ainsworth, S. Courgeon, S. J. Jorry, and H. Al-Anzi, 2013, Seismic stratigraphy of a Plio-Quaternary intra-shelf basin (Bonaparte Shelf, NW Australia): West Australian Basins Symposium 2013 Proceedings, Perth, p. 1–18.

Burchette, T., and V. Wright, 1992, Carbonate ramp depositional systems: Sedimentary Geology, v. 79, p. 3–57, <http://doi.org/10.1016/0037-0738(92)90003-A>.

Burchette, T. P., 1993, Mishrif Formation (Cenomanian-Turonian), southern Arabian Gulf: Carbonate platform growth along a cratonic basin margin, *in* J. A. T. Simo, R. W. Scott, J.–P. Masse, eds., Cretaceous carbonate platforms: American Association of Petroleum Geologists Memoir 56, Tulsa, Oklahoma, p. 185–199, <http://doi.org/10.1306/M56578C16>.

Droste, H., 1990, Depositional cycles and source rock development in an epeiric intra-platform basin: The Hanifa Formation of the Arabian Peninsula: Sedimentary Geology, v. 69, p. 281–296, <http://doi.org/10.1016/0037-0738(90)90054-W>.

Droste, H., 2010, High-resolution seismic stratigraphy of the Shu'aiba and Natih formations in the Sultanate of Oman: Implications for Cretaceous epeiric carbonate platform systems: Geological Society, London, Special Publications, v. 329, p. 145–162, <http://doi.org/10.1144/SP329.7>.

Droste, H., and M. Van Steenwinkel, 2004, Stratal geometries and patterns of platform carbonates: The Cretaceous of Oman, *in* G. P. Eberli, J. L. Masaferro, and J. F. Sarg, 2004, Seismic imaging of carbonate reservoirs and systems: American Association of Petroleum Geologists Memoir 81, Tulsa, Oklahoma, p. 185–206, <http://doi.org/10.1306/M81928>.

Dunham, R. J., 1962, Classification of carbonate rocks according to depositional textures, *in* W. E. Ham and L. C. Pray, eds., Classification of carbonate rocks—A symposium: American Association of Petroleum Geologists Memoir 1, Tulsa, Oklahoma, p. 108–121.

Eliuk, L. S., 1978, The Abenaki Formation, Nova Scotia Shelf, Canada—A depositional and diagenetic model for a Mesozoic carbonate platform: Bulletin of Canadian Petroleum Geology, v. 26, p. 424–514.

Goldhammer, R., 1991, Sequence stratigraphy and cyclostratigraphy of the Mesozoic of the Sierra Madre Oriental, northeast Mexico: A field guidebook: Gulf Coast Section of the Society of Economic Paleontologists and Mineralogists (Society for Sedimentary Geology), Houston, Texas, 85 p.

Goldhammer, R. K., 1999, Mesozoic sequence stratigraphy and paleogeographic evolution of northeast Mexico, *in* C. Bartolini, J. L. Wilson, and T. F. Lawton, eds., Mesozoic sedimentary and tectonic history of north-central Mexico: Geological Society of America Special Paper 340, Boulder, Colorado, p. 1–58.

Handford, R., and R. G. Loucks, 1993, Carbonate depositional sequences and systems tracts-responses of carbonate platforms to relative sea-level change, *in* R. G. Loucks and J. F.. Sarg, eds., Carbonate sequence stratigraphy: Recent advances and applications: American Association of Petroleum Geologists Memoir 57, Tulsa, Oklahoma, p. 3–41, <http://doi.org/10.1306/M57579C1>.

Howell, J. A., A. W. Martinius, and T. R. Good, 2014, The application of outcrop analogues in geological modelling: A review, present status and future outlook: Geological Society, London, Special Publications, v. 387, p. 1–25, <http://doi.org/10.1144/SP387.12>.

Jackson, M., and S. Seni, 1983, Geometry and evolution of salt structures in a marginal rift basin of the Gulf of Mexico, East Texas: Geology, v. 11, p. 131–135, <http://doi.org/10.1130/0091-7613(1983)11<131:GAEOSS>2.0.CO;2>.

Kerans, C., F. J. Lucia, and R. Senger, 1994, Integrated characterization of carbonate ramp reservoirs using Permian San Andres Formation outcrop analogs: American Association of Petroleum Geologists Bulletin, v. 78, p. 181–216.

Kerans, C., W. Fitchen, L. Zahm, and K. Kempter, 1995, High-frequency sequence framework of Cretaceous (Albian) carbonate ramp reservoir analog outcrops: Pecos River Canyon, northwestern Gulf of Mexico Basin: Bureau of Economic Geology Field Trip Guidebook, Austin, 105 p.

Kerans, C., and W. M. Fitchen, 1995, Sequence hierarchy and facies architecture of a carbonate-ramp system: San Andres Formation of Algerita Escarpment and western Guadalupe Mountains, West Texas and New Mexico: Bureau of Economic Geology Report of Investigations 235, Austin, 86 p.

Kerans, C., and S. W. Tinker, 1997, Sequence stratigraphy and characterization of carbonate reservoirs. Society of Economic Paleontologists and Mineralogists (Society for Sedimentary Geology) Short Course Notes 40, Tulsa, Oklahoma, 130 p.

Kerans, C., 2002, Styles of rudist buildup development along the northern margin of the Maverick Basin, Pecos River Canyon, southwest Texas: Gulf Coast Association of Geological Societies Transactions, v. 52, p. 501–516.

Lehmann, C., D. A. Osleger, and I. Montañez, 2000, Sequence stratigraphy of Lower Cretaceous (Barremian-Albian) carbonate platforms of northeastern Mexico: Regional and global correlations: Journal of Sedimentary Research, v. 70, p. 373–391 <https://doi.org/10.1306/2DC40917-0E47-11D7-8643000102C1865D>.

Lehmann, C., D. A. Osleger, and I. P. Montanez, 1998, Controls on cyclostratigraphy of Lower Cretaceous carbonates and evaporites, Cupido and Coahuila platforms, northeastern Mexico: Journal of Sedimentary Research, v. 68, p. 1109–1130, <https://doi.org/10. 2110/jsr.68.1109>.

Lozo, F., and C. Smith, 1964, Revision of Comanche Cretaceous stratigraphic nomenclature, southern Edwards Plateau, southwest Texas: Gulf Coast Association of Geological Societies Transactions: v. 14, p. 285–307.

Markello, J., and J. Read, 1981, Carbonate ramp-to-deeper shale shelf transitions of an Upper Cambrian intrashelf basin, Nolichucky Formation, southwest Virginia Appalachians: Sedimentology, v. 28, p. 573–597, <http://doi.org/10.1111/j.1365-3091.1981.tb01702.x>.

Meyer, K. M., and L. R. Kump, 2008, Oceanic euxinia in Earth history: Causes and consequences: Annual Reviews of Earth and Planetary Sciences, v. 36, p. 251–288, <http://doi.org/36.031207.124256>.

Mitchum, R. M., and J. C. Van Wagoner, 1991, High-frequency sequences and their stacking patterns: Sequence-stratigraphic evidence of high-frequency eustatic cycles: Sedimentary Geology, v. 70, p. 131–160, <http://doi.org/10.1016/0037-0738(91)90139-5>.

Osleger, D. A., R. Barnaby, and C. Kerans, 2004, A laterally accreting grainstone margin from the Albian of northern Mexico: Outcrop model for Cretaceous carbonate reservoirs, *in* G. M. Grammer, P. M. Harris, and G. P. Eberli, eds., Integration of outcrop and modern analogs in reservoir modeling: American Association of Petroleum Geologists Memoir 80, Tulsa, Oklahoma, p. 93–107, <http://doi.org/10.1306/M80924C5>.

Phelps, R. M., C. Kerans, R. O. Da-Gama, J. Jeremiah, D. Hull, and R. G. Loucks, 2015, Response and recovery of the Comanche carbonate platform surrounding multiple Cretaceous oceanic anoxic events, northern Gulf of Mexico: Cretaceous Research, v. 54, p. 117–144, <http://doi.org/10.1016/j.cretres.2014.09.002>.

Phelps, R. M., C. Kerans, R. G. Loucks, R. O. Da Gama, J. Jeremiah, and D. Hull, 2014, Oceanographic and eustatic control of carbonate platform evolution and sequence stratigraphy on the Cretaceous (Valanginian–Campanian) passive margin, northern Gulf of Mexico: Sedimentology, v. 61, p. 461–496, <http://doi.org/10.1111/sed.12062>.

Pringle, J., J. Howell, D. Hodgetts, A. Westerman, and D. Hodgson, 2006, Virtual outcrop models of petroleum reservoir analogues: A review of the current state-of-the-art: First break, v. 24, no. 3, p. 33–42.

Pringle, J., A. Westerman, J. Clark, N. Drinkwater, and A. Gardiner, 2004, 3D high-resolution digital models of outcrop analogue study sites to constrain reservoir model uncertainty: an example from Alport Castles, Derbyshire, UK: Petroleum Geoscience, v. 10, p. 343–352, <http://doi.org/10.1144/1354-079303-617>.

Razin, P., F. Taati, and F. Van Buchem, 2010, Sequence stratigraphy of Cenomanian-Turonian carbonate platform margins (Sarvak Formation) in the High Zagros, SW Iran: An outcrop reference model for the Arabian Plate: Geological Society, London, Special Publications, v. 329, p. 187–218, <http://doi.org/10.1144/SP329.9>.

Read, J. F., 1985, Carbonate platform facies models: American Association of Petroleum Geologists Bulletin, v. 69, p. 1–21, <http://doi.org/10.1130/B31442.1>.

Read, J. F., 1998, Phanerozoic carbonate ramps from greenhouse, transitional and ice-house worlds: clues from field and modelling studies: Geological Society, London, Special Publications, v. 149, p. 107–135, <http://doi.org/10.1144/GSL.SP.1999.149.01.07>.

Rose, P. R., 1972, Edwards Group, surface and subsurface, Central Texas: Bureau of Economic Geology Report of Investigations 74, Austin, 198 p., <http://doi.org/10.23867/RI0074D>.

Salvador, A., 1991, Origin and development of the Gulf of Mexico Basin: Houston Geological Society Bulletin, v. 17, p. 389–444.

Scott, R. W., and C. Kerans, 2004, Late Albian carbonate platform chronostratgraphy, Devils River Formation cycles, West Texas: *Courier Forschungsinstitut Senckenberg*, v. 247, p. 129–148.

Scott, R. W., 1990, Models and stratigraphy of mid-Cretaceous reef communities, Gulf of Mexico: Society of Economic Paleontologists and Mineralogists (Society for Sedimentary Geology) Concepts in Sedimentology and Paleontology, v. 2, 102 p.

Smith, C. I., 1981, Review of the geologic setting, stratigraphy, and facies distribution of the Lower Cretaceous in northern Mexico: Lower Cretaceous stratigraphy and structure, northern Mexico: West Texas Geological Society Publication 81–74, Midland, p. 1–27.

Smith, C. I., J. B. Brown, and F. E. Lozo, 2000, Regional stratigraphic cross sections, Comanche Cretaceous (Fredericksburg-Washita Division), Edwards and Stockton plateaus, West Texas: Interpretation of sedimentary facies, depositional cycles, and tectonics: Bureau of Economic Geology, Austin, 39 p., 6 pls., 2 appendices.

Sonnenfeld, M. D., and T. A. Cross, 1993, Volumetric partitioning and facies differentiation within the Permian upper San Andres Formation of Last Chance Canyon, Guadalupe Mountains, New Mexico, *in* R. G. Loucks and J. F.. Sarg, eds., Carbonate sequence stratigraphy: Recent advances and applications: American Association of Petroleum Geologists Memoir 57, Tulsa, Oklahoma, p. 3–41, p. 435–474, <http://doi.org/10.1306/M57579C17>.

Vail, P. R., 1987, Seismic stratigraphy interpretation using sequence stratigraphy: Part 1. Seismic stratigraphy interpretation procedure, *in* A. W. Bally, ed., Atlas of seismic stratigraphy: American Association of Petroleum Geologists Studies in Geology 27, Tulsa, Oklahoma, p. 2–14.

Van Buchem, F., B. Pittet, H. Hillgarten, J. Grotsch, A. Al-Mansouri, I. Billing, H. Droste, H. Oterdoom, and M. Van Steenwinkel, 2002a, High-resolution sequence stratigraphic architecture of the Barremian-Aptian carbonate systems in northern Oman and the United Arab Emirates Kharaib and Shu'aiba Formations: GeoArabia, v. 7, p. 461–500.

Van Buchem, F. S., P. Razin, P. W. Homewood, W. H. Oterdoom, and J. Philip, 2002b, Stratigraphic organization of carbonate ramps and organic-rich intrashelf basins: Natih Formation (middle Cretaceous) of northern Oman: American Association of Petroleum Geologists Bulletin, v. 86, p. 21–53.

Van Buchem, F. S., P. Razin, P. W. Homewood, J. M. Philip, G. P. Eberli, J.–P. Platel, J. Roger, R. Eschard, G. M. Desaubliaux, and T. Boisseau, 1996, High resolution sequence stratigraphy of the Natih Formation (Cenomanian/Turonian) in northern Oman: distribution of source rocks and reservoir facies: GeoArabia, v. 1, p. 65–91.

Van Wagoner, J. C., R. Mitchum, K. Campion, and V. Rahmanian, 1990, Siliciclastic sequence stratigraphy in well logs, cores, and outcrops: Concepts for high-resolution correlation of time and facies: American Association of Petroleum Geologists Methods in Exploration Series 7, Tulsa, Oklahoma, 55 p.

Waite, L. E., 2009, Edwards (Stuart City) shelf margin of South Texas: New data, new concepts: American Association of Petroleum Geologists Search and Discovery Article 10177, Tulsa, Oklahoma, 39 p., <http://www.searchanddiscovery.com/documents/2009/10177waite/images/waite.pdf>.

Webster, R. E., 1980, Structural Analysis of Devils River Uplift–southern Val Verde Basin, southwest Texas: American Association of Petroleum Geologists Bulletin, v. 64, p. 221–241.

Wilson, J. L., 1975, Carbonate facies in geologic history: Springer-Verlag, New York, 471 p.

Winker, C. D., and R. T. Buffler, 1988, Paleogeographic evolution of early deep-water Gulf of Mexico and margins, Jurassic to middle Cretaceous (Comanchean): American Association of Petroleum Geologists Bulletin, v. 72, p. 318–346.

Yose, L. A., A. S. Ruf, C. J. Strohmenger, J. S. Schuelke, A. Gombos, I. Al-Hosani, S. Al-Maskary, G. Bloch, Y. Al-Mehairi, and I. G. Johnson, 2006, Three-dimensional characterization of a heterogeneous carbonate reservoir, Lower Cretaceous, Abu Dhabi (United Arab Emirates), *in* P. M. Harris and L. J. Weber, eds., Giant hydrocarbon reservoirs of the world: From rocks to reservoir characterization and modeling: American Association of Petroleum Geologists Memoir 88, Tulsa, Ok-lahoma, p. 173–212, <http://doi.org/10.1306/1215877M882562>.

Zahm, L. C., 1997, Depositional model and sequence stratigraphic framework for upper Albian/lower Cenomanian carbonate ramp, western Comanche Shelf, Texas: Master's Thesis, University of Texas at Austin, 134 p.

Ziegler, M. A., 2001, Late Permian to Holocene paleofacies evolution of the Arabian Plate and its hydrocarbon occurrences: GeoArabia, v. 6, p. 445–504.